The Cryosphere, 19, 3259–3277, 2025
https://doi.org/10.5194/tc-19-3259-2025

The Cryosphere Open Access EGU

Seasonality and scenario dependence of rapid Arctic sea ice loss events in CMIP6 simulations

Annelies Sticker[1], François Massonnet[1], Thierry Fichefet[1], Patricia DeRepentigny[1], Alexandra Jahn[2,3], David Docquier[4], Christopher Wyburn-Powell[2,3], Daphne Quint[2], Erica Shivers[2], and Makayla Ortiz[2]

[1]Earth and Life Institute, Earth and Climate, UCLouvain, Louvain-la-Neuve, Belgium
[2]Department of Atmospheric and Oceanic Sciences, University of Colorado Boulder, Boulder, CO, USA
[3]Institute for Arctic and Alpine Research, University of Colorado Boulder, Boulder, CO, USA
[4]Dynamical Meteorology and Climatology Unit, Royal Meteorological Institute of Belgium, Brussels, Belgium

Correspondence: Annelies Sticker (annelies.sticker@uclouvain.be)

Received: 19 June 2024 – Discussion started: 1 July 2024
Revised: 21 May 2025 – Accepted: 2 June 2025 – Published: 26 August 2025

Abstract. The end-of-summer Arctic Ocean is projected to face at least one occurrence of practically ice-free conditions (sea ice extent $< 1 \times 10^6$ km^2) by the middle of the century under all Coupled Model Intercomparison Project Phase 6 (CMIP6) scenarios. Climate models indicate that this transition toward a practically ice-free Arctic Ocean in late summer will be punctuated by rapid ice loss events (RILEs), i.e., year-to-year reductions in total sea ice extent that occur at a much faster rate than expected from the forced contribution. The extreme sea ice loss associated with RILEs in climate models exceeds any observed rates of sea ice loss since the start of the satellite era, including the highest observed rate of -0.28×10^6 km^2 yr^{-1} during 2001–2008. As such, there could be a much faster transition toward practically ice-free conditions than expected based on a linear trend of past observations. However, RILEs are not well understood, and it is currently impossible to predict their occurrence a season to several years ahead. It is therefore essential to improve our understanding of these events. This study presents the first comprehensive analysis of RILEs in a diverse set of 26 CMIP6 models, including five large ensembles, following both low- and high-warming scenarios over the period from 1970 to 2100. Our analysis shows that RILEs are expected to occur year-round, but the timing and duration of these events are found to be season-dependent, with less frequent but longer-lived RILEs in winter and spring and more frequent but shorter-lived RILEs in summer and fall under a high-emission scenario. In addition, we find that the warming scenario has a greater influence on RILE characteristics in the winter–spring season than in the summer–fall season. Our results also emphasize that model uncertainty is larger regarding the probability and characteristics of RILEs for winter–spring events compared to summer–fall ones. Finally, while the initial sea ice extent at which RILEs are triggered depends on whether they occur in September or March, the initial sea ice volume is similar for both months, which emphasizes the critical role of sea ice thickness as a preconditioning factor for RILEs. Based on CMIP6 models, there is an approximately 60 % chance that at least one summer RILE will start in September before 2030. This study of RILEs is particularly opportune as CMIP6 models suggest that, following a period of relative stability in Arctic sea ice, the probability of a rapid sea ice reduction will increase. Given the relatively stable conditions observed between 2015 and 2024, the current summer Arctic sea ice state may have an increased probability of being on the verge of a rapid sea ice loss event.

1 Introduction

The state of the sea ice cover in the Arctic stands as an important sign of the region's transition to a warmer climate, highlighting its role as both an indicator and a driver of global change (Serreze et al., 2009; Serreze and Barry, 2011; Taylor et al., 2013; Meredith et al., 2019). Over the past few decades, the Arctic has undergone large changes, leaving the sea ice system in a new state (Landrum and Holland, 2020).

The sea ice extent (SIE) at the end of summer has diminished by 12.13 % per decade between 1979 and 2024 relative to the 1981–2010 average (Fetterer et al., 2017). The decrease in Arctic SIE occurs not only in September but also throughout the year (Onarheim et al., 2018), and in addition to the reduction in extent, the sea ice cover is much younger and thinner, making the ice that survives year-round more vulnerable to atmospheric and oceanic forcing (Stroeve and Notz, 2018).

The long-term negative trend in Arctic SIE is largely attributed to the increase in greenhouse gas concentrations in the atmosphere (Stroeve and Notz, 2015; Meredith et al., 2019). However, superimposed upon this trend is an interannual to decadal variability leading to periods of relative stability interrupted by abrupt sea ice declines (Kay et al., 2011; Swart et al., 2015; Baxter et al., 2019). As an example, Arctic sea ice retreated more than 3 times faster in the first decade of the 21st century (2001–2010: -1.7×10^6 km^2 per decade) than it did in the last 2 decades of the 20th century (1981–2000: -0.5×10^6 km^2 per decade). More recently, the September sea ice extent trend over 2012–2021 has been slightly positive (0.027×10^6 km^2 per decade).

Accelerated sea ice retreat during one or over several consecutive seasons can have profound impacts on the Arctic environment. During such periods, the accessibility of shipping routes can be greatly enhanced for several months of the year and winter sea ice might become thin enough to let light icebreakers cruise to the Arctic safely all year round (Crawford et al., 2021). Ecosystems can also feel the effects of sudden multiyear sea ice retreats, as the length of the sea ice season exerts a first-order control on the amount of light reaching phytoplankton, the building blocks of the Arctic food web (Arrigo and van Dijken, 2011; Wassmann et al., 2011). Finally, by exposing more of the Arctic Ocean to the atmosphere for several years in a row, extended periods of large sea ice decline can enhance the ice-albedo feedback and lead to increased temperature and evaporation, which could translate into extreme weather events in the terrestrial regions of the Arctic periphery (e.g., Alaska, Svalbard, and coastal Siberia; Screen et al., 2015; Delhaye et al., 2023; Lawrence et al., 2008).

Sea ice loss events are also studied on shorter timescales, with very rapid ice loss events (VRILEs) describing abrupt declines in sea ice that happen over days to weeks (e.g., Wang et al., 2020; McGraw et al., 2022; Frank, 2024). VRILEs are often associated with atmospheric and oceanic anomalies that enhance ice loss over short periods, typically within a season. While these studies have deepened our understanding of subseasonal sea ice variability, the focus of the present study is on RILEs, which manifest on subdecadal to decadal timescales.

The concept of a RILE was first proposed by Holland et al. (2006) when they identified periods of abrupt reduction in summer Arctic sea ice in seven simulations of the Community Climate System Model (CCSM) version 3. Several modeling studies on RILEs have since followed (e.g., Lawrence et al., 2008; Holland et al., 2008; Döscher and Koenigk, 2013; Paquin et al., 2013; Auclair and Tremblay, 2018; Mioduszewski et al., 2019; Rieke et al., 2023), and they all project that RILEs will become more prevalent in the upcoming decades as sea ice variability rises. Despite the previous studies on RILEs, we still currently lack a year-round overview of the properties of RILEs and the mechanisms underlying the occurrence of RILEs remain poorly understood, posing challenges in accurately predicting their onset from one season to several years in advance.

The latest generation of models participating in the Coupled Model Intercomparison Project (CMIP6) exhibits several improvements in its representation of global and polar climate. These models show a more realistic estimate of the sensitivity of September Arctic sea ice area to CO_2 emissions and improved representation of sea ice dynamics (SIMIP Community, 2020; Watts et al., 2021), making it worthwhile to reassess Arctic sea ice variability through the lens of RILEs. In this study, we present the first investigation of RILEs year-round using a multimodel ensemble gathering 26 different climate models as well as five large ensembles (Sect. 2). The impact of different emission scenarios is also evaluated using two future Shared Socioeconomic Pathways (SSPs): a low-emission scenario (SSP1-2.6) and a high-emission scenario (SSP5-8.5). We first assess the seasonality of RILEs, highlighting large differences in the characteristics of RILEs that occur in the first versus last 6 months of the year (Sect. 3.1). We also look at the probability of RILEs in CMIP6 simulations (Sect. 3.2). Then we focus on the timing of RILEs as well as the SIE and total sea ice volume (SIV) at which RILEs start, focusing on September and March RILEs (Sect. 3.3). Finally, we discuss the implications of our results and draw conclusions in Sects. 4 and 5.

2 Data and methods

2.1 Data

We analyze data from the first ensemble member of 26 CMIP6 models (see Table 1) that were chosen based on the availability of the sea ice variable SIE, sea ice concentration (SIC), and SIV. The nominal horizontal resolution of the ocean or sea ice component from the different CMIP6 models varies between 25 and 250 km, with the majority using a resolution of 100 km (Table 1). We use output from historical simulations, which cover the period 1850 to 2014, except for the EC-Earth3 large ensemble spanning the period from 1970 to 2014. We also employed two sets of climate projections following low- and high-warming scenarios, specifically SSP1-2.6 and SSP5-8.5, which correspond to top-of-atmosphere radiative forcings in 2100 of 2.6 and 8.5 W m^{-2} with respect to preindustrial levels (O'Neill et al., 2016). Under SSP1-2.6, the Arctic SIE continues to decline in the earlier decades of the 21st century before stabilizing towards the

latter part of the century (Fig. S1 in the Supplement). The climate projections cover the period 2015 to 2100, except for the CAMS-CSM1-0 model (model no. 4 in Table 1), which ranges from 2015 to 2099. We only use the years covered by all models and, as such, our study focuses on the time period 1970–2099.

In addition to the CMIP6 multimodel ensemble that allows for a detailed investigation of model uncertainty, we analyze historical and SSP5-8.5 simulations from five large ensembles to better understand the role of internal climate variability in our results: ACCESS-ESM1.5 (40 ensemble members; Ziehn et al., 2020), CanESM5 (25 ensemble members; Swart et al., 2019d), EC-Earth3 (50 ensemble members; Wyser et al., 2021), MIROC6 (50 ensemble members; Shiogama et al., 2023), and MPI-ESM1.2-LR (30 ensemble members; Olonscheck et al., 2023). These large ensembles and their ensemble size were chosen based on the availability of sea ice variables. Using multiple large ensembles offers a robust comparison of forced responses and internal climate variability across models (Deser et al., 2020).

The primary sea ice output used in this study is the Arctic SIE, labeled *siextentn* in the CMIP6 output. In cases where *siextentn* was unavailable, we computed the SIE time series using the SIC data, labeled *siconc* in the CMIP6 output. SIE is calculated as the total area of all grid cells where SIC exceeds 15 %. SIE is a commonly used metric for model comparisons (Shu et al., 2020; Watts et al., 2021; Shen et al., 2021), and our choice of SIE metrics aligns with the existing definitions of RILEs to maintain consistency (Auclair and Tremblay, 2018). However, it is important to note that a limitation of SIE compared to sea ice area (SIA), as highlighted by Notz (2014), is its strong dependency on grid resolution. Additionally, changes in SIA can occur with relatively little change in SIE, which suggests that RILEs defined in terms of SIA may represent fundamentally different processes than those defined using SIE. Nonetheless, we find that our conclusions using SIE are generally consistent with results using SIA (not shown). We also analyzed SIV, labeled *sivoln* in the CMIP6 output. If SIV was not available, we computed the total Arctic SIV from sea ice thickness (SIT), labeled *sivol* (grid-cell-averaged ice thickness) or *sithick* (sea ice thickness averaged over the ice-covered portion of a grid cell) in the CMIP6 output. When only *sithick* was provided, we calculated SIV by multiplying *sithick* by SIC and the grid cell area. By taking into account the vertical dimension, the SIV metric offers a more comprehensive representation of the condition of the Arctic sea ice cover as it relates more directly to the thermodynamic processes governing its evolution (Stroeve and Notz, 2015).

2.2 Model evaluation

Climate models are powerful tools for analyzing the mean state, trends, and variability of the climate system and how these will evolve in the future. However, the reliability of the conclusions related to sea ice drawn from modeling studies is dependent on the accuracy of the representation of Arctic sea ice and the underlying physical processes embedded within models. To ensure the robustness of our results, we evaluate the performance of the sea ice simulations used in this study with the newly developed SITool (Lin et al., 2021). This tool is designed to assess the skill of CMIP6 simulations by comparing various sea ice metrics with observational references. To do so, we rely on observations of SIE and SIC obtained from the NASA Team (NSIDC-0051) dataset (Cavalieri et al., 1996) and reanalysis of SIT from PIOMAS (Schweiger et al., 2011). Observed SIC and SIT reanalysis data are available from 1979 and, as such, the evaluation of CMIP6 models focuses on the period 1979 to 2014.

SITool reveals noticeable differences between models of the multimodel ensemble in their representation of SIE (Fig. S2 in the Supplement); however, the multimodel mean demonstrates good performance relative to observational data for both March and September (Fig. 1a). Additionally, we find that the majority of CMIP6 models effectively replicate the mean and variability of SIC, SIE, and SIT as well as the spatial distribution of the ice edge (Figs. S2 and S3 in the Supplement). Note that some models exhibit larger disparities in one or more metrics when compared to observed references: BCC-CSM2-MR, CAMS-CSM1-0, NESM3, EC-Earth3, and MIROC-E2SL. However, we find that screening out these models does not affect our conclusions (not shown) and, therefore, we have retained this subset of models for the analysis. We also conducted the same evaluation of all members of the five large ensembles for SIE and found that ACCESS-ESM1.5 and MPI-ESM1.2-LR demonstrate better performance in reproducing the mean state, standard deviation, and trend of Arctic sea ice extent, while CanESM5, EC-Earth3, and MIROC6 show slightly lower performance (Figs. 1b and S4 in the Supplement). Specifically, CanESM5 exhibits a particularly negative trend during 1979 to 2014 compared to observations, and MIROC6 shows a less negative trend compared to observations (Fig. S5 in the Supplement) and greatly underestimates SIE from November to June (Bianco et al., 2024; Tatebe et al., 2019).

2.3 Definition of RILEs

Several definitions exist in the scientific literature for RILEs in the Arctic, each emphasizing distinct criteria and temporal characteristics (Holland et al., 2008; Lawrence et al., 2008; Döscher and Koenigk, 2013; Paquin et al., 2013; Auclair and Tremblay, 2018; Mioduszewski et al., 2019; Rieke et al., 2023). Holland et al. (2006) used the rate of change exceeding a specific threshold, determined through the derivative of the 5-year mean smoothed time series of SIE. Based on this definition, a RILE is identified when sea ice loss surpasses $0.5 \times 10^6\,\mathrm{km^2\,yr^{-1}}$, with the event's duration based on the period during which SIE decreases by more than $0.15 \times 10^6\,\mathrm{km^2\,yr^{-1}}$. In contrast, Auclair and Tremblay (2018) de-

Table 1. Ocean and sea ice components, together with their nominal resolution, of the CMIP6 models used in this analysis. The resolution corresponds to the ocean or sea ice component. The sea ice component for models 19–20 is unnamed but uses the "Semtner zero-layer" thermodynamic and "Hibler 79" dynamic schemes.

Model name	Ocean model	Sea ice model	Ocean or sea ice resolution
1. ACCESS-CM2	MOM5	CICE5.1.2	100 km
2. ACCESS-ESM1.5	MOM5	CICE 4.1	100 km
3. BCC-CSM2-MR	MOM4	SIS2	50 km
4. CAMS-CSM1-0	MOM4	SIS1.0	100 km
5. CESM2-WACCM	POP 2	CICE 5.1	100 km
6. CESM2	POP 2	CICE 5.1	100 km
7. CNRM-CM6-1-HR	NEMO 3.6	Gelato 6.1	25 km
8. CNRM-CM6-1	NEMO 3.6	Gelato 6.1	100 km
9. CNRM-ESM2-1	NEMO 3.6	Gelato 6.1	100 km
10. CanESM5	NEMO3.4.1	LIM2	100 km
11. EC-Earth3-Veg	NEMO 3.6	NEMO-LIM3	100 km
12. EC-Earth3	NEMO 3.6	NEMO-LIM3	100 km
13. GFDL-ESM4	GFDL-OM4p5	GFDL-SIM4p5	50 km
14. HadGEM3-GC31-LL	NEMO-HadGEM3-GO6.0	CICE-HadGEM3-GSI8	100 km
15. HadGEM3-GC31-MM	NEMO-HadGEM3-GO6.0	CICE-HadGEM3-GSI8	25 km
16. IPSL-CM6A-LR	NEMO 3.6	NEMO-LIM 3	100 km
17. MIROC-ES2L	COCO4.9	COCO4.9	100 km
18. MIROC6	COCO4.9	COCO4.9	100 km
19. MPI-ESM1.2-HR	MPIOMI 1.6.3	Unnamed	50 km
20. MPI-ESM1.2-LR	MPIOMI 1.6.3	Unnamed	250 km
21. MRI-ESM2-0	MRI.COM 4.4	MRI.COM 4.4	100 km
22. NESM3	NEMO v3.4	CICE4.1	100 km
23. NorESM2-LM	MICOM	CICE	100 km
24. NorESM2-MM	MICOM	CICE	100 km
25. TaiESM1	POP2	CICE4	50 km
26. UKESM1-0-LL	NEMO-HadGEM3-GO6.0	CICE-HadGEM3-GS18	100 km

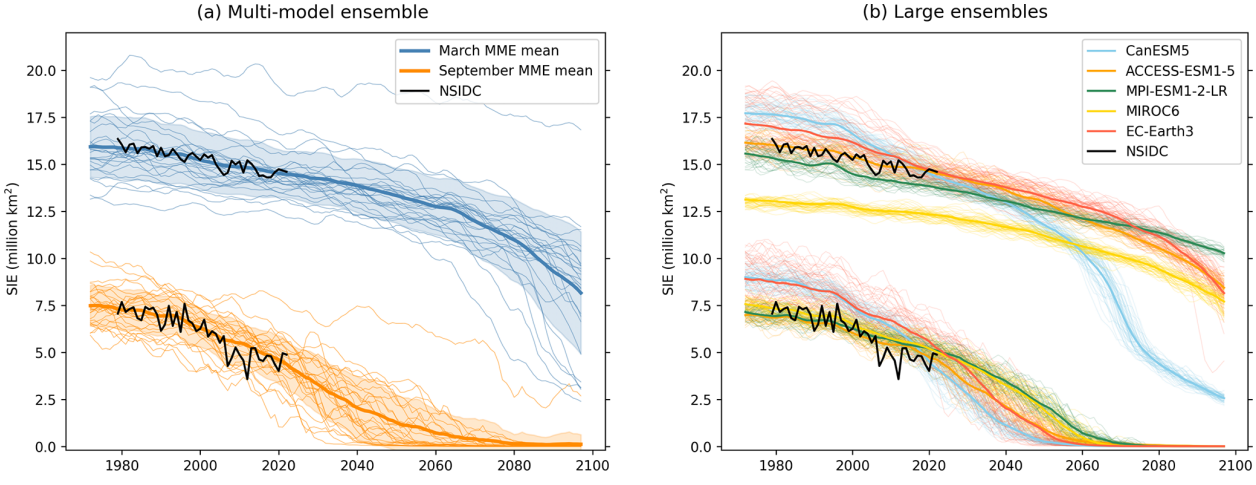

Figure 1. March (top lines) and September (bottom lines) 5-year running mean SIE evolution over the historical period and the high-emission scenario SSP5-8.5 for **(a)** the CMIP6 multimodel ensemble (26 models, one member per model), with thin lines representing individual models, thick lines the multimodel ensemble mean, and shaded areas 1 standard deviation across the multimodel ensemble. **(b)** Five large ensembles with thin lines representing individual ensemble members and thick lines representing the ensemble mean. The black lines show the observations from NSIDC.

fined rapid sea ice declines based on a period lasting at least 4 years, with the trend in the 5-year running mean minimum SIE consistently lower than or equal to $-0.3 \times 10^6\,\mathrm{km^2\,yr^{-1}}$. Döscher and Koenigk (2013) characterized a RILE as a drop in summer SIE exceeding $1.2 \times 10^6\,\mathrm{km^2}$. According to their definition, a RILE can manifest itself as a single large drop ("one-step event") or a series of up to three consecutive steps involving smaller year-to-year drops ("multiyear event"). Finally, Rieke et al. (2023) assessed rapid ice change events in the Barents Sea using 5-year linear trends of winter (November–April) SIA and the criteria of trends exceeding 2 standard deviations of the distribution of 5-year trends in the Community Earth System Model Large Ensemble (CESM-LE) between 2007 and 2025.

For this study, we use the definition of Auclair and Tremblay (2018), for which a RILE is a period lasting at least 4 years, during which the trend in the 5-year running mean minimum SIE is lower than or equal to $-0.3 \times 10^6\,\mathrm{km^2\,yr^{-1}}$. We chose this definition as it emphasizes the total amount of loss during a RILE, with the 5-year running mean filtering out interannual variability, and it limits RILEs to events that last several years rather than single-year events, thus focusing on events with a higher impact on climate, ecosystems, and society. We apply the definition of Auclair and Tremblay (2018) to all months of the year, maintaining the same threshold. According to this definition, a RILE is even more extreme than the most rapid observed sea ice loss to date. Indeed, over the period 1979–2024, the observed SIE in the Arctic decreased by $0.037 \times 10^6\,\mathrm{km^2\,yr^{-1}}$ in March and by $0.078 \times 10^6\,\mathrm{km^2\,yr^{-1}}$ in September (Fetterer et al., 2017), with the most rapid sea ice decline in September over the period 2001–2008 reaching $-0.28 \times 10^6\,\mathrm{km^2\,yr^{-1}}$.

3 Results

3.1 Seasonality of RILEs

When examining the occurrence of RILEs throughout the year from 1970 to 2099, we find a distinct regime difference between the first and last 6 months of the year (Figs. 2 and 3). Indeed, the characteristics of RILEs (e.g., the total number of RILEs simulated, duration over multiple years, and intraseasonal consistency over several months during 1 year) are noticeably different between winter–spring and summer–fall RILEs under both the high- and low-warming scenarios (Fig. 2). From January to June, very few RILEs are simulated by the CMIP6 multimodel ensemble between 1970 and 2050, with an increasing frequency toward the end of the 21st century under the high-warming scenario (SSP5-8.5) in about one-third of the models (Fig. 2a and b). These winter and spring RILEs also exhibit intraseasonal consistency, meaning that they extend over multiple months of the same year (see the darker colors in Fig. 2a and b). For the low-warming scenario (SSP1-2.6), only a few RILEs are simulated over the 130 years of our study period, indicating a large contribution from scenario uncertainty to the probability of occurrence of future winter and spring RILEs (Figs. 2e and f and 4a). In contrast, between July and December, RILEs are more abundant, though more short-lived, and appear to be randomly distributed throughout the time period when sea ice is present (1970 to consistently ice-free conditions; Jahn et al., 2024; Senftleben et al., 2020) for both warming scenarios (Fig. 2c, d, g, and h). We also see a smaller impact of the choice of future scenario on RILEs occurring in the last 6 months of the year, especially for summer RILEs (July–August–September; Fig. 2c and g). This suggests that forcing factors predominantly influence winter and spring conditions, with little to no role in summer–fall conditions.

This regime difference between winter and summer RILEs is also present in the large ensembles (Fig. 3). Additionally, we see a large contribution of model uncertainty to the probability of occurrence of future winter RILEs (Fig. 3a–e), something that is also apparent in the CMIP6 multimodel ensemble under a high-warming scenario (Fig. 2a and b). Model uncertainty is reflected in the timing when winter RILEs first occur as well as their intraseasonal consistency for multiple months of the year (Fig. 3). In Sect. 3.3, we take a closer look at some important characteristics of RILEs that will shed light on the physical processes leading to this model uncertainty.

While the overall pattern reveals an increase in RILE occurrence from late spring through winter, differences emerge across the models (Fig. 5a). The CanESM5 large ensemble displays a relatively uniform distribution of RILEs throughout the year, with an average number of RILEs per simulation ranging from 2 in March/April to 2.7 in October. In contrast, the EC-Earth3, ACCESS-ESM1.5, MIROC6, and MPI-ESM1.2-LR large ensembles exhibit more pronounced seasonal variability, with a higher occurrence of RILEs from late spring to early winter. The RILE seasonal patterns for the EC-Earth3 and ACCESS-ESM1.5 large ensembles resemble that of the CMIP6 multimodel ensemble for the SSP5-8.5 scenario (Fig. 4a). On the other hand, the MIROC6 and MPI-ESM1.2-LR large ensembles exhibit a seasonality pattern in RILE similar to the CMIP6 SSP1-2.6 multimodel distribution, even though all large-ensemble analyses here are based on the SSP5-8.5 scenario. The occurrence of RILEs in MIROC6, being similar to the RILE occurrence in the multimodel ensemble under the SSP1-2.6 scenario despite the stronger forcing of the SSP5-8.5 scenario, can be attributed to the relatively weak long-term SIE trend in MIROC6, as shown in Fig. S5. However, the comparison between ACCESS-ESM1.5 and MPI-ESM1.2-LR further underscores the complexity: while the SIE values in both models show similarly weak SIE trends, they differ in their RILE seasonality. This suggests that, while the long-term SIE trend plays a role in determining the seasonality of RILE occurrence, other factors – such as the mean state and internal variability – are also important. For instance, SIE in ACCESS-

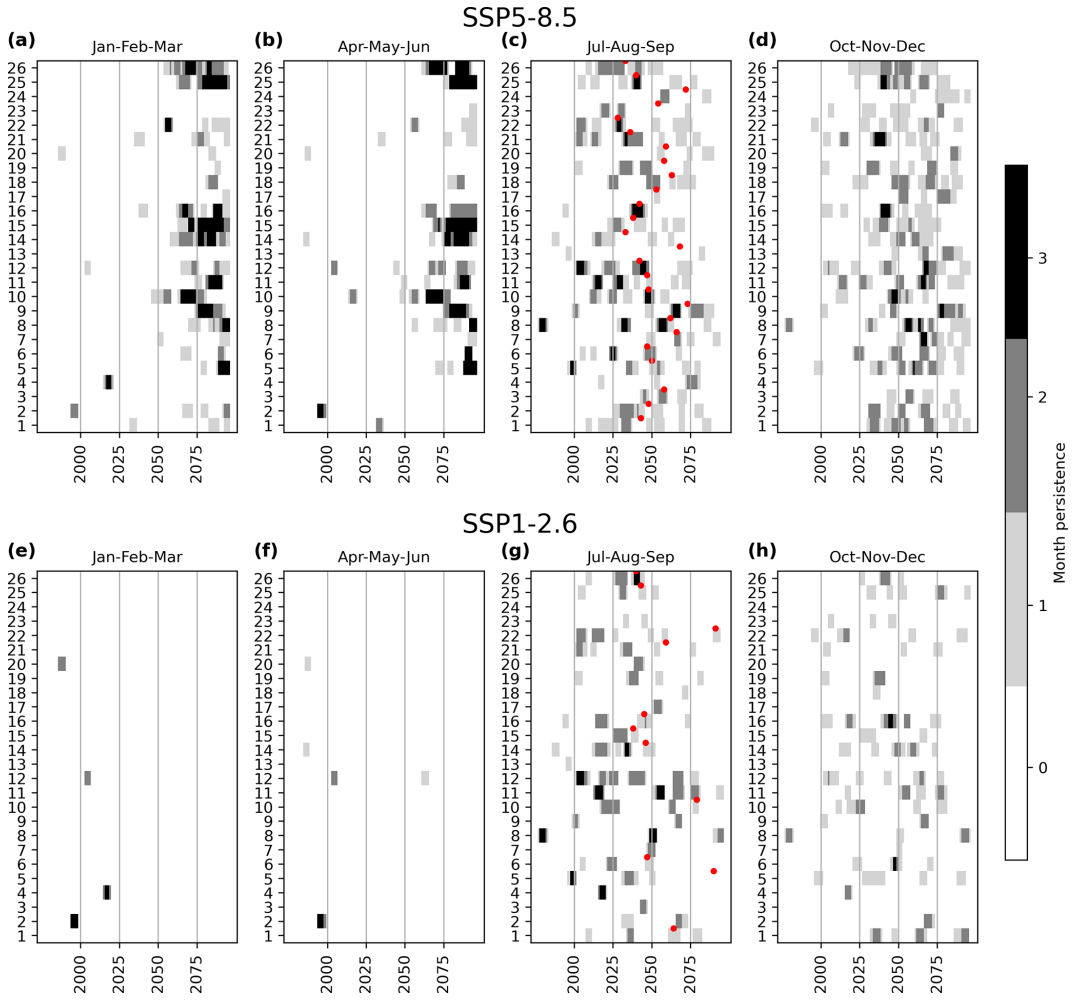

Figure 2. Occurrences of RILEs from 1970 to 2099 in the first ensemble member of the 26 different CMIP6 models following the SSP5-8.5 **(a–d)** and SSP1-2.6 **(e–h)** scenarios. Each panel shows a period of 3 months, with light grey representing RILEs occurring over 1 of the 3 months, dark grey representing RILEs occurring over 2 of the 3 months, and black representing RILEs occurring over all 3 months of the season. The numbers on the *y* axis refer to the 26 different models listed in Table 1. The red dots in the July–August–September panels indicate the first year of consistently ice-free conditions in September (i.e., the first year of 5 consecutive years when the smoothed September SIE falls below 1×10^6 km^2).

ESM1.5 has a higher internal variability than MPI-ESM1.2-LR but a similar mean state (Fig. 6), which likely contributes to the differences in their seasonal distributions.

Because of the expected increase in sea ice variability as the thickness of the ice cover decreases (Holland et al., 2008) as well as the extreme sea ice loss associated with RILEs, one could expect an early transition toward consistently ice-free conditions in models that simulate many RILEs. However, we find no clear relationship between RILE occurrence and the timing of consistently ice-free conditions in September, with instances of September ice-free conditions occurring at the end of multiple, few, or no RILEs at all. Indeed, some models from the five large ensembles simulate many RILEs before reaching consistently ice-free conditions in September (e.g., CanESM5, EC-Earth3, and ACCESS-ESM1.5), while others simulate only a few if any (e.g., MIROC6 and MPI-ESM1.2-LR; Fig. 3). We also find that some models start simulating winter RILEs immediately after the occurrence of consistently ice-free conditions in September (e.g., CanESM5), while for other models (e.g., ACCESS-ESM1.5, MIROC6, and EC-Earth3) there is a lag of around 20–30 years between the timing of consistently ice-free conditions in September and the onset of winter RILEs. Additionally, some models simulate a large number of winter RILEs across all ensemble members (CanESM5, ACCESS-ESM1.5, and EC-Earth3), whereas only a few winter RILEs are simulated for MPI-ESM1.2-LR and no RILE is simulated in March for MIROC6 (Fig. 5a). This confirms that uncertainty regarding the initiation of winter RILEs is

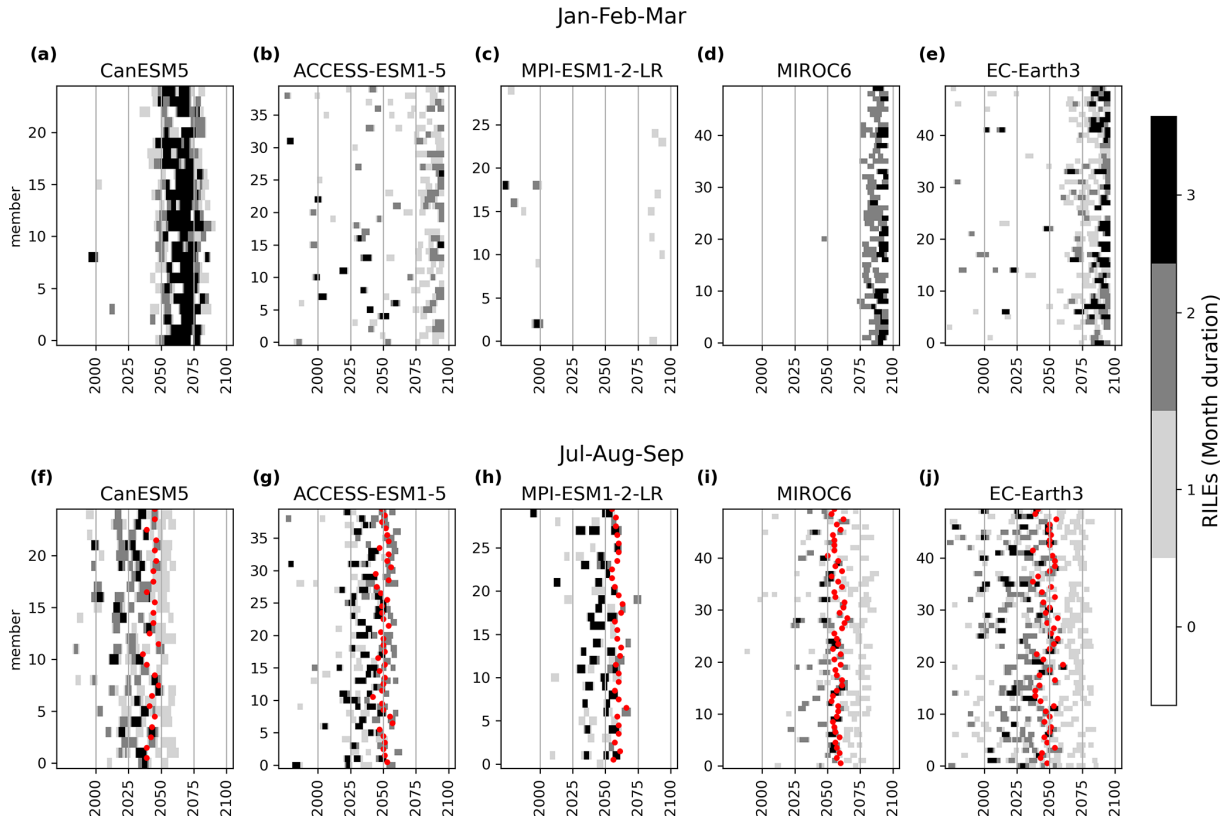

Figure 3. Same as in Fig. 2 but for the periods January–February–March **(a–e)** and July–August–September **(f–j)** in the five large ensembles following the SSP5-8.5 scenario.

large and strongly model-dependent in addition to the choice of future scenario, as discussed above.

According to the CMIP6 multimodel ensemble, around 50 % of September RILEs (SRILEs) end at a SIE value under 2×10^6 km^2 and 30 % between 0 and 1×10^6 km^2 (i.e., consistently ice-free conditions) for both warming scenarios (Fig. 8d). This is also the case for the large ensembles: 18 %–37 % of the SRILEs end below the 1×10^6 km^2 threshold (Fig. 9d). For MIROC6, the majority of SRILEs have a SIE at around 2.5×10^6 km^2 at their onset, which is the lowest value compared to other large ensembles (Fig. 9b). Accordingly, 37 % of MIROC6 SRILEs end at a SIE below 1×10^6 km^2 (Fig. 9d). While the timing of consistently ice-free conditions in September shows little correlation with the occurrence of RILEs, long-lasting SRILEs can directly lead to ice-free conditions, although such events are relatively rare. Specifically, RILEs lasting more than 10 years frequently result in ice-free conditions, but these extended events account for less than 15 % of all RILEs across both the multimodel ensembles and large ensembles. Indeed, most SRILEs typically persist for 4 to 6 years (Figs. 4b and 5b). Moreover, this pattern appears consistent across models, suggesting that SRILE duration is not strongly model-dependent.

3.2 Probability of occurrence of RILEs

The probability of having at least one SRILE over the period 1970–2099 in the CMIP6 multimodel ensemble is 92 % for both scenarios, with a maximum of five SRILEs projected during this period for one single simulation (Fig. 4c). When looking at results from the large ensembles, we find disparities across models in terms of the probability of occurrence of SRILEs. There is a 78 % probability of having at least one SRILE per simulation with the MIROC6 large ensemble, with 46 % of the simulations having only one RILE over the period 1970–2099. In contrast, the EC-Earth3 large ensemble shows a 100 % probability of having at least one SRILE over the same period, with 90 % of the simulations projected to have more than one SRILE (Fig. 5c). This range of results may be related to differences in SIE mean state, variability, and trends among models (Figs. 1 and 6). This again highlights the important role of model uncertainty and the models' mean state in the probability of occurrence of RILEs.

The percentage of simulations exhibiting a RILE before 2030 was analyzed with the multimodel ensemble under both scenarios (SSP1-2.6 and SSP5-8.5) and large ensembles for the SSP5-8.5 scenario (Figs. 4d and 5d). Approximately 60 % of the simulations show a SRILE before 2030, with intermodel differences in the probability. MIROC6 shows a

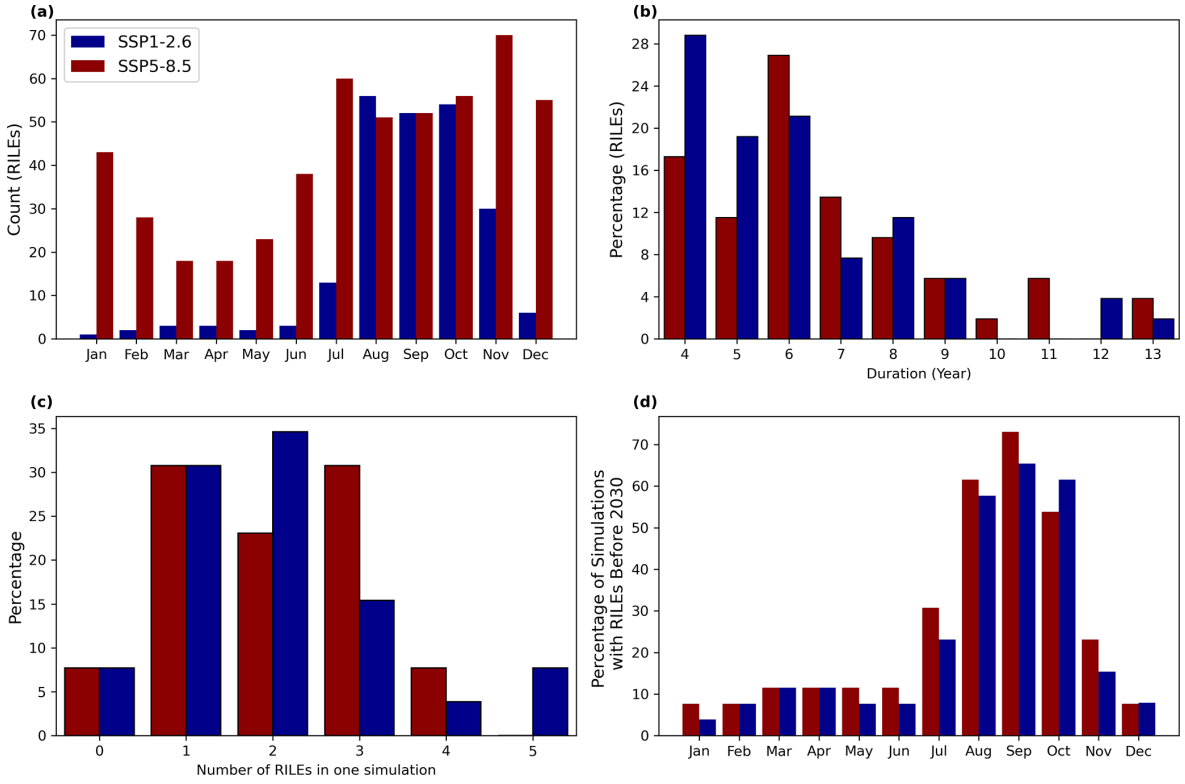

Figure 4. RILE characteristics in the CMIP6 multimodel ensemble. **(a)** Total number of RILEs per month, **(b)** percentage of SRILEs as a function of their duration in years, **(c)** percentage of SRILEs per simulation, and **(d)** percentage of simulations with at least one RILE occurrence before 2030 in each month for the CMIP6 multimodel ensemble over 1970–2099 under the high-warming (red) and low-warming (blue) scenarios.

minimum of 26 %, while CanESM5 reaches 92 %, highlighting strong intermodel variability. This large range of probabilities across models shows that a large sea ice model spread remains a concern for CMIP6 models and that analyzing multiple models is crucial for best characterizing the uncertainty inherent in current sea ice projections. While systematic biases in CMIP6 models remain a concern – models can reproduce current sea ice trends for incorrect levels of global warming, as shown by Rosenblum and Eisenman (2017) for CMIP5 models – our results provide insights by relying on a multimodel ensemble of 26 models and five large ensembles. As the forcings for the SSP5-8.5 and SSP1-2.6 scenarios remain comparable until 2030, the probability of RILEs occurring before 2030 is similar across multiple models under both the SSP5-8.5 and SSP1-2.6 scenarios. The analysis of large ensembles reveals that models with high SRILE occurrences before 2030 (80 %–92 %; i.e., CanESM5, ACCESS-ESM1.5, and EC-Earth3) also exhibit increased variability in sea ice extent starting in the late 2010s (Fig. 6a). This enhanced variability increases the likelihood of RILEs before 2030. In contrast, models with lower variability (MIROC6 and MPI-ESM1-2) and an underestimated mean sea ice extent in March (Fig. 1) show a lower (26 %–30 %) probability of SRILE occurrence before 2030. While the different SIE interannual variability in models influences the probability of RILEs, their occurrences remain more frequent in summer than in winter, especially from August to October, stabilizing around 60 % in the multimodel ensemble (Fig. 4d). Outside the summer season, this probability decreases sharply but does not drop to 0 % for the multimodel ensemble, indicating that RILEs, although less frequent, could still occur before 2030 during other months of the year as well. However, there is a clear model dependence in the seasonal distribution of RILEs. For instance, MIROC6 does not project any RILEs before 2030 outside the summer months, suggesting a strong seasonal confinement in this model.

Interestingly, we find an increased probability of SRILE occurrence after a period of no sea ice loss (i.e., a 10-year period with a neutral or positive SIE trend; Fig. 7). Indeed, while the overall probability of a RILE occurring in the multimodel ensemble from 2015 until consistently ice-free conditions under SSP5-8.5 is 7 %, the likelihood increases to around 20 % following a period of no sea ice loss. This increase in probability after a decade of neutral or positive trends is consistent across the CMIP6 multimodel ensemble (Fig. 7) and the five large ensembles (Fig. S7 in the Supplement), and those differences are all highly significant (z score > 5). In addition, the SIV trend during the 10-year

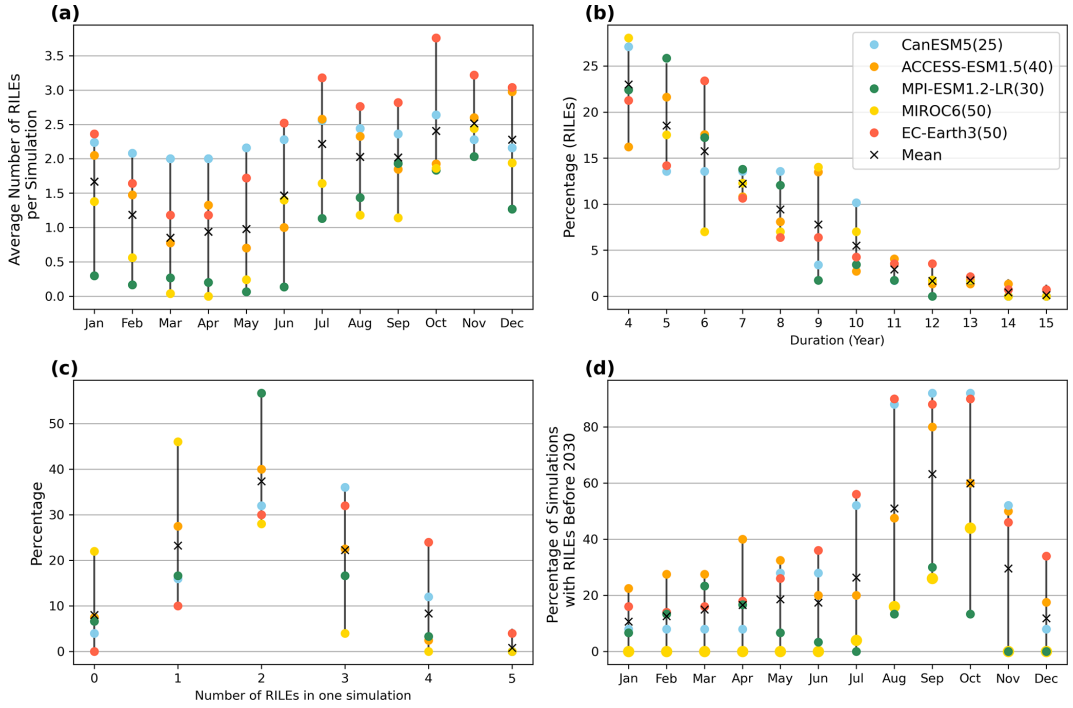

Figure 5. RILE characteristics in five large ensembles following the high-emission SSP5-8.5 scenario. **(a)** Average number of RILEs per simulation per month. **(b–d)** Same as Fig. 4. The black "X" represents the mean across the five large ensembles, and the numbers in parentheses in the legend indicate the ensemble size for each large ensemble.

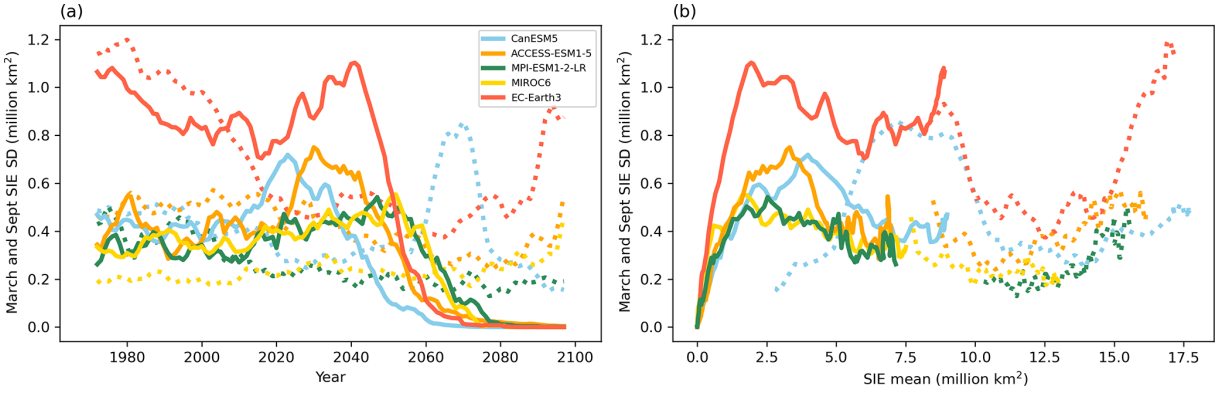

Figure 6. Standard deviation of the 5-year running mean SIE for March (dotted lines) and September (solid lines) as a function of **(a)** time. **(b)** September and March SIE mean state for the five large ensembles following the high-emission scenario SSP5-8.5.

period of no trend or a positive trend does not increase the probability of a RILE occurring in the subsequent years (not shown).

3.3 Mean state influence on RILE occurrence

SRILEs start occurring in the late 20th century and early 2000s for the CMIP6 multimodel ensemble (Fig. 8a). By 2025, 50 % of SRILEs have already occurred, and by 2070 all events have taken place for both scenarios. For the large ensembles, the initiation of SRILEs is similar to the CMIP6 multimodel ensemble: 50 % of the total number of SRILEs have already occurred at the earliest by year 2020, as in CanESM5, and at the latest by 2040 for models such as MIROC6 and MPI-ESM1.2-LR (Fig. 9a). In these models, the timing of SRILEs is consistent with an increase in September SIE variability (Holland et al., 2008): sea ice variability in CanESM5 starts to increase around 2010 and peaks around 2025, whereas the peak in SIE variability for MIROC6 and MPI-ESM1.2-LR occurs about 20 years later (Fig. 6a).

Even though the timing of SRILEs varies by up to 2 decades across models, the peak probability of RILE onset as

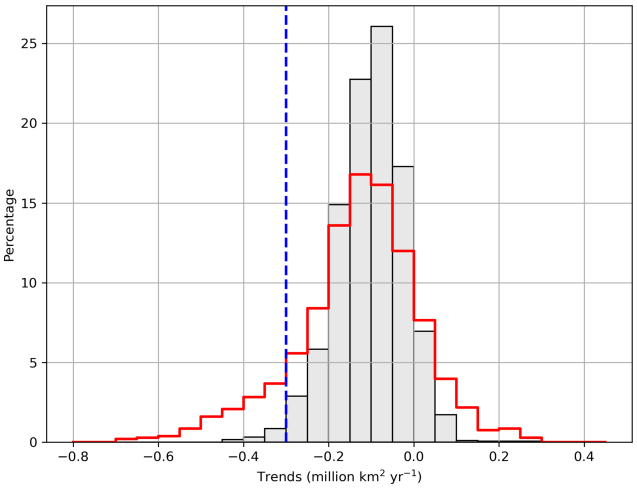

Figure 7. Distribution of all possible 10-year Arctic September SIE trends (grey) and trends after a period of stability (red) for the CMIP6 multimodel ensemble from 2015 to consistently ice-free conditions using the SSP5-8.5 scenario. A period of stability is defined as a 10-year period with a neutral or positive SIE trend. The 10-year trends are computed on the 5-year running mean SIE time series. The dotted blue line indicates the threshold used to define a RILE (see Sect. 2.3 for more details). Figure S7 shows similar results but for the five large ensembles.

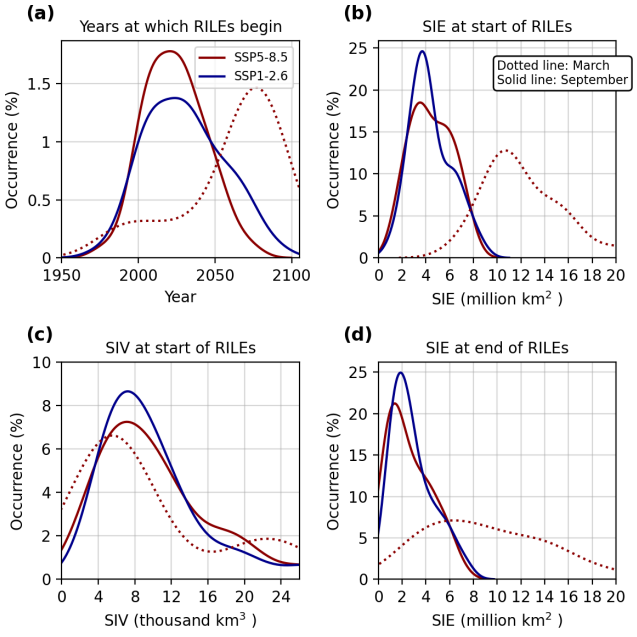

Figure 8. RILE characteristics in the CMIP6 multimodel ensemble: probability density function of the **(a)** years, **(b)** SIE and **(c)** SIV at which RILEs begin, and **(d)** SIE at which RILEs end for September (solid lines) and March (dotted lines) for the CMIP6 multimodel ensemble over 1970–2099 under the high-warming (red) and low-warming (blue) scenarios. Note that we do not show results for the low-warming scenario in March due to very few RILEs being simulated.

a function of SIE is quite consistent for both the CMIP6 multimodel ensemble and large ensembles at slightly less than 4×10^6 km^2 (Figs. 8b and 9b), which suggests that the dependence of RILE onset on the mean state is similar across models. This is also the SIE at which the large ensembles simulate the largest values of September sea ice variability (Fig. 6). EC-Earth3 and CanESM5 show a double peak distribution for SIE at the end of SRILEs (Fig. 9b and d), which is consistent with early and late RILEs due to high sea ice variability for EC-Earth3 and the early increase in variability (2010–2015) for CanESM5 (Fig. 6).

In contrast to September, March RILE (MRILE hereafter) occurrences are mostly simulated after 2050. The peak MRILE occurrence is around 2075 and for SIE values around 11×10^6 km^2 in the CMIP6 multimodel ensemble following the high-warming scenario (Fig. 8a and b). Of the large ensembles simulating MRILEs (i.e., EC-Earth3, CanESM5, and ACCESS-ESM1.5), the mean SIE at the onset of MRILEs is similar to the CMIP6 multimodel ensemble, except for ACCESS-ESM1.5, for which the peak in MRILE occurrences is around 15×10^6 km^2 (Fig. 9b). Uncertainty in the timing of MRILEs is more pronounced across these large ensembles (Fig. 9a), highlighting once more the large contribution of model uncertainty to winter RILEs. This uncertainty can be explained by differences in sea ice mean state and/or variability. For example, although the onset years for winter RILEs differ between CanESM5 and EC-Earth3 (Fig. 9a), both large ensembles show an increase in sea ice variability as the March SIE falls below 10×10^6 km^2 (Fig. 6). In contrast, MPI-ESM1.2-LR exhibits much lower March sea ice variability as a function of both time and SIE (Fig. 6), resulting in few winter RILEs (Fig. 5a). Both ACCESS-ESM1.5 and MIROC6 show an increase in sea ice variability over the last few decades of the 21st century as they reach a lower SIE (Fig. 6), resulting in an increase in the occurrence of winter RILEs at that time (Fig. 3). The probability density functions of SIE at the end of MRILEs are flatter and wider than the ones for SRILEs (Figs. 8d and 9d), which is explained by the large contribution of model uncertainty to the initial SIE as well as the duration and intraseasonal consistency of MRILEs.

A peak of RILE occurrences between 5000 and 7500 km^3 of SIV is evident for both September and March (Fig. 8c) in the CMIP6 multimodel ensemble. This parity in the probability of the initial SIV between September and March suggests that the average ice volume state may serve as preconditioning for RILE occurrences. Indeed, we find that more than 20 % of SRILEs begin at a SIV ranging from 4000 to 6000 km^3. The declining mean state of SIV likely drives the similarity in SIV at the onset of SRILEs and MRILEs. By 2060–2080, reduced winter SIV (mean: 9.75×10^3 km^3 in March) approaches early-21st-century summer values (mean: 8.23×10^3 km^3 in September 2000–2020), in-

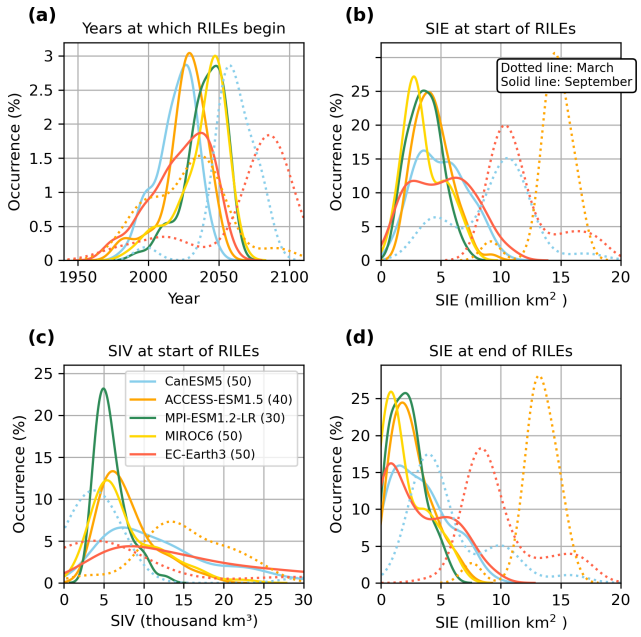

Figure 9. Same as Fig. 8 but for the five large ensembles following the high-emission scenario SSP5-8.5. The numbers in parentheses in the legend indicate the ensemble size for each large ensemble. Note that we do not show results for MPI-ESM1.2-LR and MIROC6 in March due to very few MRILEs being simulated in these two models.

dicating that future winters will resemble today's summers and contribute to RILEs in all seasons (Fig. S8 in the Supplement). Additionally, SIV differs between these periods: March SIV in 2060–2080 shows lower interannual variability (mean SD $\approx 1.5 \times 10^3$ km^3) than September SIV in 2000–2020 (mean SD $\approx 2.0 \times 10^3$ km^3, range 0.5–4.5 $\times 10^3$ km^3). This greater summer variability suggests that occasional high summer SIV values in the early 21st century can match low winter SIV levels in the middle to late 21st century.

It is important to note that reaching a critical sea ice state is not a sufficient condition for winter RILEs to occur. MIROC6 simulates no winter RILEs before the last 2 decades of the 21st century (Fig. 3d) despite showing a less extensive and thinner winter ice cover (Figs. 1b and S6b in the Supplement). Holland et al. (2008) showed that, in addition to a forcing perturbation, an adequately thin ice cover is necessary to initiate RILEs in September, and our results suggest that this finding is also applicable to winter RILEs, except for EC-Earth3. Indeed, EC-Earth3 simulates winter RILEs at the end of the 20th century (Fig. 3e) without meeting the thin sea ice condition.

4 Discussion

The increase in RILE occurrence follows the increase in SIE variability, echoing previous findings regarding the influence of large interannual SIE fluctuations on abrupt Arctic SIE declines (Holland et al., 2008; Goosse et al., 2009). This variability is highest when approaching consistently ice-free conditions (Swart et al., 2015; Mioduszewski et al., 2019), with increased SIE variability in summer and fall attributed to the higher efficiency of open-water formation, while variability in November–January is influenced by ice growth (Mioduszewski et al., 2019). Increased variability in SIE has been found to be linked to declining ice thickness (Holland et al., 2008), particularly in winter, with a complex interplay between climate, ice thickness, and geographical factors (Goosse et al., 2009; Mioduszewski et al., 2019). Our results also suggest a preconditioning role of SIV in RILEs, as similar SIV values are observed at the onset of SRILEs and MRILEs. At first, this may seem surprising since winter SIV is generally expected to be larger than summer SIV (e.g., as shown in PIOMAS time series). However, this similarity can be explained by two factors. First, there is large interannual variability in September SIV, so that anomalously high summer SIV values can occasionally match mid- to late-21st-century winter SIV values. Second, March RILEs occur later in the 21st century, when March SIV has declined to levels comparable to late-20th-century September SIV. Both interpretations influence the preconditioning role of the SIV, but the declining mean state of the sea ice volume seems to be the dominant factor. However, while the total SIV may reach similar values, sea ice spatial distributions will differ. Present-day summer sea ice consists of thicker, multiyear ice in a small area (north of the Canadian Arctic Archipelago and Greenland – where ice survives the summer melt), whereas mid- to late-century winter sea ice will likely be thinner, with first-year sea ice covering most of the Arctic Ocean. These differences imply distinct responses to events that could trigger RILEs. According to Döscher and Koenigk (2013), RILEs are controlled by the initial SIV at the onset of the melting period and by the onset of specific atmospheric circulation patterns during summer months. In summer months, thinning ice cover in climate models increases ice extent variability, making it more vulnerable to natural variations, amplifying changes due to the surface albedo feedback, and resulting in an increased probability of extreme events such as RILEs.

Based on the analyzed CMIP6 model simulations, our study suggests that the most probable occurrence of a SRILE would be in the mid-2020s, or once we reach September SIE and SIV mean states of approximately 3.5×10^6 km^2 and 6000 km^3, respectively. By comparison, the observed September mean SIE over the past 5 years (2020–2024) was approximately 4.52×10^6 km^2 (Fetterer et al., 2017), while the September mean SIV over the past 5 years was approximately 4600 km^3 (Schweiger et al., 2011). As such, the current sea ice state (SIE and SIV) is close to the projected characteristics of SRILEs in CMIP6 simulations. Additionally, the increased probability of SRILE occurrence after a period of no sea ice loss (Fig. 7) suggests that the proba-

Table 2. References for the different CMIP6 simulations under the various scenarios used in this study.

Model name	Reference historical simulations	Reference SSP5-8.5 simulations	Reference SSP1-2.6 simulations
1. ACCESS-CM2	Dix et al. (2019a)	Dix et al. (2019c)	Dix et al. (2019b)
2. ACCESS-ESM1.5	Ziehn et al. (2019a)	Ziehn et al. (2019c)	Ziehn et al. (2019b)
3. BCC-CSM2-MR	Wu et al. (2018)	Xin et al. (2019b)	Xin et al. (2019a)
4. CAMS-CSM1-0	Rong (2019c)	Rong (2019b)	Rong (2019a)
5. CESM2-WACCM	Danabasoglu (2019d)	Danabasoglu (2019f)	Danabasoglu (2019e)
6. CESM2	Danabasoglu (2019a)	Danabasoglu (2019c)	Danabasoglu (2019b)
7. CNRM-CM6-1-HR	Voldoire (2019a)	Voldoire (2019b)	Voldoire (2020)
8. CNRM-CM6-1	Voldoire (2018)	Voldoire (2019d)	Voldoire (2019c)
9. CNRM-ESM2-1	Seferian (2018)	Voldoire (2019f)	Voldoire (2019e)
10. CanESM5	Swart et al. (2019a)	Swart et al. (2019c)	Swart et al. (2019b)
11. EC-Earth3-Veg	EC-Earth-Consortium (2019d)	EC-Earth-Consortium (2019f)	EC-Earth-Consortium (2019e)
12. EC-Earth3	EC-Earth-Consortium (2019a)	EC-Earth-Consortium (2019c)	EC-Earth-Consortium (2019b)
13. GFDL-ESM4	Krasting et al. (2018)	John et al. (2018b)	John et al. (2018a)
14. HadGEM3-GC31-LL	Ridley et al. (2019a)	Good (2020b)	Good (2020a)
15. HadGEM3-GC31-MM	Ridley et al. (2019b)	Jackson (2020b)	Jackson (2020a)
16. IPSL-CM6A-LR	Boucher et al. (2018)	Boucher et al. (2019b)	Boucher et al. (2019a)
17. MIROC-ES2L	Hajima et al. (2019)	Tachiiri et al. (2019b)	Tachiiri et al. (2019a)
18. MIROC6	Tatebe and Watanabe (2018)	Shiogama et al. (2019b)	Shiogama et al. (2019a)
19. MPI-ESM1.2-HR	Jungclaus et al. (2019)	Schupfner et al. (2019b)	Schupfner et al. (2019a)
20. MPI-ESM1.2-LR	Wieners et al. (2019c)	Wieners et al. (2019b)	Wieners et al. (2019a)
21. MRI-ESM2-0	Yukimoto et al. (2019a)	Yukimoto et al. (2019c)	Yukimoto et al. (2019b)
22. NESM3	Cao and Wang (2019)	Cao (2019b)	Cao (2019a)
23. NorESM2-LM	Seland et al. (2019a)	Seland et al. (2019c)	Seland et al. (2019b)
24. NorESM2-MM	Bentsen et al. (2019a)	Bentsen et al. (2019c)	Bentsen et al. (2019b)
25. TaiESM1	Lee and Liang (2020a)	Lee and Liang (2020c)	Lee and Liang (2020b)
26. UKESM1-0-LL	Tang et al. (2019)	Good et al. (2019b)	Good et al. (2019a)

bility of seeing a RILE in the near future following the recent weak negative trend of observed SIE over 2015–2024 ($-0.017 \times 10^6\,\mathrm{km^2\,yr^{-1}}$; Fetterer et al., 2017) has increased, echoing previously proposed ideas of slowing down as an early warning signal for abrupt climate change (Dakos et al., 2008). This convergence emphasizes the increasing urgency to understand the variability, causes, and impacts of such events. It is important to note, however, that the exact timing and mean state associated with the occurrence of a RILE in the future are still uncertain due to the large contribution of internal climate variability. A deeper examination of the physical mechanisms driving decadal SIE variability in model simulations, through the study of RILEs in the future, is therefore crucial for enhancing our capacity to understand and predict the evolution of Arctic sea ice in the coming years and decades.

5 Conclusions

Rapid ice loss events (RILEs) were first identified by Holland et al. (2006) and, even though several follow-up studies have been conducted (Lawrence et al., 2008; Holland et al., 2008; Döscher and Koenigk, 2013; Paquin et al., 2013; Auclair and Tremblay, 2018; Mioduszewski et al., 2019; Rieke et al., 2023), we still currently lack a comprehensive overview of the properties of RILEs. Previous studies used a limited number of climate models or mainly focused on one season. Our study assessed RILEs in the Arctic in the past and future during all months of the year using a large set of realizations from five large ensembles and simulations from 26 models participating in CMIP6. The findings illustrate the complex variability of the Arctic sea ice cover through the study of RILEs, shifting from a relatively stable condition in the 20th century to a more unpredictable state as we progress further into the 21st century, especially during summer. Below, we provide a summary of the key results.

- Under a high-emission scenario (SSP5-8.5), RILEs occur in the CMIP6 multimodel ensemble (26 models) and five large ensembles for all months of the year (Figs. 2 and 3). All five large ensembles have at least one ensemble member exhibiting a RILE in every month of the year, except for MIROC6 in April. The percentage of CMIP6 models experiencing at least one RILE varies depending on the month of the year, ranging from 62 % (February to May) to 96 % (August and November).
- The large number of RILEs simulated by the CMIP6 multimodel ensemble in August, September, and October is similar across both future scenarios, but this is not the case over the rest of the year (November–

July), with significantly fewer RILEs when using the low-emission scenario (SSP1-2.6; Fig. 4a). This suggests that the choice of forcing has little influence on the probability of occurrence of end-of-summer RILEs but plays a dominant role in all other months of the year.

- RILEs in winter last longer than in summer and tend to occur toward the end of the century under SSP5-8.5, while they are almost nonexistent toward the end of the century in climate projections using SSP1-2.6 (Fig. 2). During the last 6 months of the year, RILEs are more randomly spread than during the first 6 months of the year, indicating a regime difference between different times of the year. Additionally, it seems that there is a larger influence of model uncertainty on the timing of RILEs in winter.
- The increase in RILE occurrence is driven by the increase in SIE variability (Fig. 6), as already highlighted by Holland et al. (2008) in their analysis of rapid September sea ice retreat. Our results suggest that this finding is also applicable to winter RILEs. On top of that, the greater the sea ice extent variability is in a model, the more the model simulates RILEs. This result is most clearly illustrated by EC-Earth3 (large ensemble), in which there is a high probability (90 %) of experiencing more than one RILE (two to five) during the period from 1970 to consistently ice-free conditions.
- SIV values at the onset of RILEs are similar for both March and September RILEs and both scenarios in the CMIP6 multimodel analysis (Fig. 8c). This suggests a preconditioning role of SIV for RILEs, with a threshold ranging from 5000 to 7500 km^3.
- There is an increase in the probability that a RILE will occur after a 10-year steady SIE phase (Fig. 7). This increases the probability of a RILE in the near future, following the weak negative SIE trend period between 2015 and 2024 ($-0.017 \times 10^6\,km^2\,yr^{-1}$).

To conclude, RILEs can happen in any month of the year, not just during summer, depending on future emission scenarios. Given how frequently RILEs occur in climate models, the rapid loss of sea ice that a RILE entails should not come as a surprise if it were to happen in reality.

Code and data availability. The data from all of the CMIP6 models are openly available and can be found on the Earth System Grid Federation (ESGF) nodes at https://esgf-node.ipsl.upmc.fr/search/cmip6-ipsl/ (WCRP, 2025). The DOI (digital object identifier) for each model simulation can be found in Table 2. The PIOMAS (Schweiger et al., 2011) sea ice volume data can be accessed via the Polar Science Center of the University of Washington at http://psc.apl.uw.edu/research/projects/arctic-sea-ice-volume-anomaly/data/ (Polar Science Center, 2025; Zhang and Rothrock, 2003). The observational SIE data from the National Snow and Ice Data Center (NSIDC) can be accessed at https://doi.org/10.5067/IJ0T7HFHB9Y6 (Stroeve and Meier, 2018).

Supplement. The supplement related to this article is available online at https://doi.org/10.5194/tc-19-3259-2025-supplement.

Author contributions. AS, FM, TF, and AJ conceptualized the science plan. AS performed the analyses, produced the figures, and wrote the manuscript based on the insights from the co-authors. AS, PDR, AJ, FM, DD, and TF contributed to the writing, reviewing, and editing. Initial analyses of the seasonality of RILEs and the SIE threshold where RILEs begin to occur were performed on a subset of a large ensemble by DQ, ES, and MO, respectively, under guidance from CWP and AJ.

Competing interests. The contact author has declared that none of the authors has any competing interests.

Disclaimer. The views and opinions expressed are those of the author(s) only and do not necessarily reflect those of the European Union or the European Research Council Executive Agency. Neither the European Union nor the granting authority can be held responsible for them.

Publisher's note: Copernicus Publications remains neutral with regard to jurisdictional claims made in the text, published maps, institutional affiliations, or any other geographical representation in this paper. While Copernicus Publications makes every effort to include appropriate place names, the final responsibility lies with the authors.

Acknowledgements. Annelies Sticker and Patricia DeRepentigny are funded by the European Commission, European Research Council (ArcticWATCH, grant no. 101040858). François Massonnet is a Fond de la Recherche Scientifique de Belgique (F.R.S.–FNRS) Research Associate. David Docquier is funded by BELSPO through the RESIST project (contract no. RT/23/RESIST). Computational resources have been provided by the supercomputing facilities of the Université catholique de Louvain (CISM/UCL) and the Consortium des Équipements de Calcul Intensif en Fédération Wallonie Bruxelles (CÉCI) funded by F.R.S.–FNRS under convention 2.5020.11. The contributions of Alexandra Jahn, Christopher Wyburn-Powell, Daphne Quint, Erica Shivers, and Makayla Ortiz were supported by NSF-CAREER award no. 1847398. We acknowledge the World Climate Research Programme's Working Group on Coupled Modelling, which is responsible for CMIP, and we thank the climate modeling groups for producing and making available their model output. We acknowledge the use of ChatGPT (https://chat.openai.com/, last access: 31 May 2025) to improve the writing style of a few paragraphs.

Financial support. Annelies Sticker and Patricia DeRepentigny are funded by the European Commission, European Research Council (ArcticWATCH, grant no. 101040858). François Massonnet is a Fond de la Recherche Scientifique de Belgique (F.R.S.– FNRS) Research Associate. David Docquier is funded by BELSPO through the RESIST project (contract no. RT/23/RESIST). The contributions of Alexandra Jahn, Christopher Wyburn-Powell, Daphne Quint, Erica Shivers, and Makayla Ortiz were supported by NSF-CAREER award no. 1847398.

Review statement. This paper was edited by Jari Haapala and reviewed by two anonymous referees.

References

Arrigo, K. and van Dijken, G.: Secular trends in Arctic Ocean net primary production, J. Geophys. Res.-Oceans, 116, C09011, https://doi.org/10.1029/2011JC007151, 2011.

Auclair, G. and Tremblay, L. B.: The Role of Ocean Heat Transport in Rapid Sea Ice Declines in the Community Earth System Model Large Ensemble, J. Geophys. Res.-Oceans, 123, 8941–8957, https://doi.org/10.1029/2018JC014525, 2018.

Baxter, I., Ding, Q., Schweiger, A., L'Heureux, M., Baxter, S., Wang, T., Zhang, Q., Harnos, K., Markle, B., Topal, D., and Lu, J.: How Tropical Pacific Surface Cooling Contributed to Accelerated Sea Ice Melt from 2007 to 2012 as Ice Is Thinned by Anthropogenic Forcing, J. Climate, 32, 8583–8602, https://doi.org/10.1175/JCLI-D-18-0783.1, 2019.

Bentsen, M., Oliviè, D. J. L., Seland, Ø., Toniazzo, T., Gjermundsen, A., Graff, L. S., Debernard, J. B., Gupta, A. K., He, Y., Kirkevåg, A., Schwinger, J., Tjiputra, J., Aas, K. S., Bethke, I., Fan, Y., Griesfeller, J., Grini, A., Guo, C., Ilicak, M., Karset, I. H. H., Landgren, O. A., Liakka, J., Moseid, K. O., Nummelin, A., Spensberger, C., Tang, H., Zhang, Z., Heinze, C., Iversen, T., and Schulz, M.: NCC NorESM2-MM model output prepared for CMIP6 CMIP historical, https://doi.org/10.22033/ESGF/CMIP6.8040, 2019a.

Bentsen, M., Oliviè, D. J. L., Seland, Ø., Toniazzo, T., Gjermundsen, A., Graff, L. S., Debernard, J. B., Gupta, A. K., He, Y., Kirkevåg, A., Schwinger, J., Tjiputra, J., Aas, K. S., Bethke, I., Fan, Y., Griesfeller, J., Grini, A., Guo, C., Ilicak, M., Karset, I. H. H., Landgren, O. A., Liakka, J., Moseid, K. O., Nummelin, A., Spensberger, C., Tang, H., Zhang, Z., Heinze, C., Iversen, T., and Schulz, M.: NCC NorESM2-MM model output prepared for CMIP6 ScenarioMIP ssp126, https://doi.org/10.22033/ESGF/CMIP6.8250, 2019b.

Bentsen, M., Oliviè, D. J. L., Seland, Ø., Toniazzo, T., Gjermundsen, A., Graff, L. S., Debernard, J. B., Gupta, A. K., He, Y., Kirkevåg, A., Schwinger, J., Tjiputra, J., Aas, K. S., Bethke, I., Fan, Y., Griesfeller, J., Grini, A., Guo, C., Ilicak, M., Karset, I. H. H., Landgren, O. A., Liakka, J., Moseid, K. O., Nummelin, A., Spensberger, C., Tang, H., Zhang, Z., Heinze, C., Iversen, T., and Schulz, M.: NCC NorESM2-MM model output prepared for CMIP6 ScenarioMIP ssp585, https://doi.org/10.22033/ESGF/CMIP6.8321, 2019c.

Bianco, E., Blanchard-Wrigglesworth, E., Materia, S., Ruggieri, P., Iovino, D., and Masina, S.: CMIP6 Models Underestimate Arctic Sea Ice Loss during the Early Twentieth-Century Warming, despite Simulating Large Low-Frequency Sea Ice Variability, J. Climate, 37, 6305–6321, https://doi.org/10.1175/JCLI-D-23-0647.1, 2024.

Boucher, O., Denvil, S., Levavasseur, G., Cozic, A., Caubel, A., Foujols, M.-A., Meurdesoif, Y., Cadule, P., Devilliers, M., Ghattas, J., Lebas, N., Lurton, T., Mellul, L., Musat, I., Mignot, J., and Cheruy, F.: IPSL IPSL-CM6A-LR model output prepared for CMIP6 CMIP historical, https://doi.org/10.22033/ESGF/CMIP6.5195, 2018.

Boucher, O., Denvil, S., Levavasseur, G., Cozic, A., Caubel, A., Foujols, M.-A., Meurdesoif, Y., Cadule, P., Devilliers, M., Dupont, E., and Lurton, T.: IPSL IPSL-CM6A-LR model output prepared for CMIP6 ScenarioMIP SSP126, https://doi.org/10.22033/ESGF/CMIP6.5262, 2019a.

Boucher, O., Denvil, S., Levavasseur, G., Cozic, A., Caubel, A., Foujols, M.-A., Meurdesoif, Y., Cadule, P., Devilliers, M., Dupont, E., and Lurton, T.: IPSL IPSL-CM6A-LR model output prepared for CMIP6 ScenarioMIP SSP585, https://doi.org/10.22033/ESGF/CMIP6.5271, 2019b.

Cao, J.: NUIST NESMv3 model output prepared for CMIP6 ScenarioMIP SSP126, https://doi.org/10.22033/ESGF/CMIP6.8780, 2019a.

Cao, J.: NUIST NESMv3 model output prepared for CMIP6 ScenarioMIP SSP585, https://doi.org/10.22033/ESGF/CMIP6.8790, 2019b.

Cao, J. and Wang, B.: NUIST NESMv3 model output prepared for CMIP6 CMIP historical, https://doi.org/10.22033/ESGF/CMIP6.8769, 2019.

Cavalieri, D. J., Parkinson, C. L., Gloersen, P., and Zwally, H. J.: Sea Ice Concentrations from Nimbus-7 SMMR and DMSP SSM/I-SSMIS Passive Microwave Data, Version 1, https://doi.org/10.5067/8GQ8LZQVL0VL, 1996.

Crawford, A., Stroeve, J., Smith, A., and Jahn, A.: Arctic open-water periods are projected to lengthen dramatically by 2100, Communications Earth and Environment, 2, 109, https://doi.org/10.1038/s43247-021-00183-x, 2021.

Dakos, V., Scheffer, M., Van Nes, E. H., Brovkin, V., Petoukhov, V., and Held, H.: Slowing down as an early warning signal for abrupt climate change, P. Natl. Acad. Sci. USA, 105, 14308–14312, 2008.

Danabasoglu, G.: NCAR CESM2 model output prepared for CMIP6 CMIP historical, https://doi.org/10.22033/ESGF/CMIP6.7627, 2019a.

Danabasoglu, G.: NCAR CESM2 model output prepared for CMIP6 ScenarioMIP SSP126, https://doi.org/10.22033/ESGF/CMIP6.7746, 2019b.

Danabasoglu, G.: NCAR CESM2 model output prepared for CMIP6 ScenarioMIP SSP585, https://doi.org/10.22033/ESGF/CMIP6.7768, 2019c.

Danabasoglu, G.: NCAR CESM2-WACCM model output prepared for CMIP6 CMIP historical, https://doi.org/10.22033/ESGF/CMIP6.10071, 2019d.

Danabasoglu, G.: NCAR CESM2-WACCM model output prepared for CMIP6 ScenarioMIP SSP126, https://doi.org/10.22033/ESGF/CMIP6.10100, 2019e.

Danabasoglu, G.: NCAR CESM2-WACCM model output prepared for CMIP6 ScenarioMIP SSP585, https://doi.org/10.22033/ESGF/CMIP6.10115, 2019f.

Delhaye, S., Msadek, R., Fichefet, T., Massonnet, F., and Terray, L.: Consistent but more intense atmospheric circulation response to Arctic sea ice loss in CMIP6 experiments compared to PAMIP experiments, EGUsphere [preprint], https://doi.org/10.5194/egusphere-2023-1748, 2023.

Deser, C., Lehner, F., Rodgers, K., Ault, T., Delworth, T., DiNezio, P., Fiore, A., Frankignoul, C., Fyfe, J., Horton, D., Kay, J., Knutti, R., Lovenduski, N., Marotzke, J., McKinnon, K., Minobe, S., Randerson, J., Screen, J., Simpson, I., and Ting, M.: Insights from Earth system model initial-condition large ensembles and future prospects, Nat. Clim. Change, 10, 277–286, https://doi.org/10.1038/s41558-020-0731-2, 2020.

Dix, M., Bi, D., Dobrohotoff, P., Fiedler, R., Harman, I., Law, R., Mackallah, C., Marsland, S., O'Farrell, S., Rashid, H., Srbinovsky, J., Sullivan, A., Trenham, C., Vohralik, P., Watterson, I., Williams, G., Woodhouse, M., Bodman, R., Dias, F. B., Domingues, C. M., Hannah, N., Heerdegen, A., Savita, A., Wales, S., Allen, C., Druken, K., Evans, B., Richards, C., Ridzwan, S. M., Roberts, D., Smillie, J., Snow, K., Ward, M., and Yang, R.: CSIRO-ARCCSS ACCESS-CM2 model output prepared for CMIP6 CMIP historical, https://doi.org/10.22033/ESGF/CMIP6.4271, 2019a.

Dix, M., Bi, D., Dobrohotoff, P., Fiedler, R., Harman, I., Law, R., Mackallah, C., Marsland, S., O'Farrell, S., Rashid, H., Srbinovsky, J., Sullivan, A., Trenham, C., Vohralik, P., Watterson, I., Williams, G., Woodhouse, M., Bodman, R., Dias, F. B., Domingues, C. M., Hannah, N., Heerdegen, A., Savita, A., Wales, S., Allen, C., Druken, K., Evans, B., Richards, C., Ridzwan, S. M., Roberts, D., Smillie, J., Snow, K., Ward, M., and Yang, R.: CSIRO-ARCCSS ACCESS-CM2 model output prepared for CMIP6 ScenarioMIP SSP126, https://doi.org/10.22033/ESGF/CMIP6.4319, 2019b.

Dix, M., Bi, D., Dobrohotoff, P., Fiedler, R., Harman, I., Law, R., Mackallah, C., Marsland, S., O'Farrell, S., Rashid, H., Srbinovsky, J., Sullivan, A., Trenham, C., Vohralik, P., Watterson, I., Williams, G., Woodhouse, M., Bodman, R., Dias, F. B., Domingues, C. M., Hannah, N., Heerdegen, A., Savita, A., Wales, S., Allen, C., Druken, K., Evans, B., Richards, C., Ridzwan, S. M., Roberts, D., Smillie, J., Snow, K., Ward, M., and Yang, R.: CSIRO-ARCCSS ACCESS-CM2 model output prepared for CMIP6 ScenarioMIP SSP585, https://doi.org/10.22033/ESGF/CMIP6.4332, 2019c.

Döscher, R. and Koenigk, T.: Arctic rapid sea ice loss events in regional coupled climate scenario experiments, Ocean Sci., 9, 217–248, https://doi.org/10.5194/os-9-217-2013, 2013.

EC-Earth-Consortium: EC-Earth-Consortium EC-Earth3 model output prepared for CMIP6 CMIP historical, https://doi.org/10.22033/ESGF/CMIP6.4700, 2019a.

EC-Earth-Consortium: EC-Earth-Consortium EC-Earth3 model output prepared for CMIP6 ScenarioMIP SSP126, https://doi.org/10.22033/ESGF/CMIP6.4874, 2019b.

EC-Earth-Consortium: EC-Earth-Consortium EC-Earth3 model output prepared for CMIP6 ScenarioMIP SSP585, https://doi.org/10.22033/ESGF/CMIP6.4912, 2019c.

EC-Earth-Consortium: EC-Earth-Consortium EC-Earth3-Veg model output prepared for CMIP6 CMIP historical, https://doi.org/10.22033/ESGF/CMIP6.4706, 2019d.

EC-Earth-Consortium: EC-Earth-Consortium EC-Earth3-Veg model output prepared for CMIP6 ScenarioMIP SSP126, https://doi.org/10.22033/ESGF/CMIP6.4876, 2019e.

EC-Earth-Consortium: EC-Earth-Consortium EC-Earth3-Veg model output prepared for CMIP6 ScenarioMIP SSP585, https://doi.org/10.22033/ESGF/CMIP6.4914, 2019f.

Fetterer, F., Knowles, K., Meier, W., Savoie, M., and Windnagel, A.: Sea Ice Index, Version 3 [monthly values from 1979 to 2023], https://doi.org/10.7265/N5K072F8, 2017.

Frank, M.: Driving Mechanisms of Very Rapid Sea Ice Loss Events, PhD thesis, University of Oklahoma, Norman, Oklahoma, https://hdl.handle.net/11244/340422 (last access: 11 August 2025), 2024.

Good, P.: MOHC HadGEM3-GC31-LL model output prepared for CMIP6 ScenarioMIP SSP126, https://doi.org/10.22033/ESGF/CMIP6.10849, 2020a.

Good, P.: MOHC HadGEM3-GC31-LL model output prepared for CMIP6 ScenarioMIP SSP585, https://doi.org/10.22033/ESGF/CMIP6.10901, 2020b.

Good, P., Sellar, A., Tang, Y., Rumbold, S., Ellis, R., Kelley, D., and Kuhlbrodt, T.: MOHC UKESM1.0-LL model output prepared for CMIP6 ScenarioMIP SSP126, https://doi.org/10.22033/ESGF/CMIP6.6333, 2019a.

Good, P., Sellar, A., Tang, Y., Rumbold, S., Ellis, R., Kelley, D., and Kuhlbrodt, T.: MOHC UKESM1.0-LL model output prepared for CMIP6 ScenarioMIP SSP585, https://doi.org/10.22033/ESGF/CMIP6.6405, 2019b.

Goosse, H., Arzel, O., Bitz, C. M., de Montety, A., and Vancoppenolle, M.: Increased variability of the Arctic summer ice extent in a warmer climate, Geophys. Res. Lett., 36, L23702, https://doi.org/10.1029/2009GL040546, 2009.

Hajima, T., Abe, M., Arakawa, O., Suzuki, T., Komuro, Y., Ogura, T., Ogochi, K., Watanabe, M., Yamamoto, A., Tatebe, H., Noguchi, M. A., Ohgaito, R., Ito, A., Yamazaki, D., Ito, A., Takata, K., Watanabe, S., Kawamiya, M., and Tachiiri, K.: MIROC MIROC-ES2L model output prepared for CMIP6 CMIP historical, https://doi.org/10.22033/ESGF/CMIP6.5602, 2019.

Holland, M. M., Bitz, C. M., and Tremblay, B.: Future abrupt reductions in the summer Arctic sea ice, Geophys. Res. Lett., 33, L23503, https://doi.org/10.1029/2006GL028024, 2006.

Holland, M. M., Bitz, C. M., Tremblay, L.-B., and Bailey, D. A.: The Role of Natural Versus Forced Change in Future Rapid Summer Arctic Ice Loss, American Geophysical Union (AGU), 133–150, https://doi.org/10.1029/180GM10, 2008.

Jackson, L.: MOHC HadGEM3-GC31-MM model output prepared for CMIP6 ScenarioMIP SSP126, https://doi.org/10.22033/ESGF/CMIP6.10850, 2020a.

Jackson, L.: MOHC HadGEM3-GC31-MM model output prepared for CMIP6 ScenarioMIP SSP585, https://doi.org/10.22033/ESGF/CMIP6.10902, 2020b.

Jahn, A., Holland, M. M., and Kay, J. E.: Projections of an ice-free Arctic Ocean, Nat. Rev. Earth Environ., 5, 164–176, 2024.

John, J. G., Blanton, C., McHugh, C., Radhakrishnan, A., Rand, K., Vahlenkamp, H., Wilson, C., Zadeh, N. T., Dunne, J. P., Dussin, R., Horowitz, L. W., Krasting, J. P., Lin, P., Malyshev, S., Naik, V., Ploshay, J., Shevliakova, E., Silvers, L., Stock, C., Winton, M., and Zeng, Y.: NOAA-GFDL GFDL-ESM4 model output prepared for CMIP6 ScenarioMIP SSP126, https://doi.org/10.22033/ESGF/CMIP6.8684, 2018a.

John, J. G., Blanton, C., McHugh, C., Radhakrishnan, A., Rand, K., Vahlenkamp, H., Wilson, C., Zadeh, N. T., Dunne, J. P., Dussin, R., Horowitz, L. W., Krasting, J. P., Lin, P., Malyshev, S., Naik, V., Ploshay, J., Shevliakova, E., Silvers, L., Stock, C., Winton, M., and Zeng, Y.: NOAA-GFDL GFDL-ESM4 model output prepared for CMIP6 ScenarioMIP SSP585, https://doi.org/10.22033/ESGF/CMIP6.8706, 2018b.

Jungclaus, J., Bittner, M., Wieners, K.-H., Wachsmann, F., Schupfner, M., Legutke, S., Giorgetta, M., Reick, C., Gayler, V., Haak, H., de Vrese, P., Raddatz, T., Esch, M., Mauritsen, T., von Storch, J.-S., Behrens, J., Brovkin, V., Claussen, M., Crueger, T., Fast, I., Fiedler, S., Hagemann, S., Hohenegger, C., Jahns, T., Kloster, S., Kinne, S., Lasslop, G., Kornblueh, L., Marotzke, J., Matei, D., Meraner, K., Mikolajewicz, U., Modali, K., Müller, W., Nabel, J., Notz, D., Peters-von Gehlen, K., Pincus, R., Pohlmann, H., Pongratz, J., Rast, S., Schmidt, H., Schnur, R., Schulzweida, U., Six, K., Stevens, B., Voigt, A., and Roeckner, E.: MPI-M MPI-ESM1.2-HR model output prepared for CMIP6 CMIP historical, https://doi.org/10.22033/ESGF/CMIP6.6594, 2019.

Kay, J., Holland, M., and Jahn, A.: Inter-annual to multi-decadal Arctic sea ice extent trends in a warming world, Geophys. Res. Lett., 38, L15708, https://doi.org/10.1029/2011GL048008, 2011.

Krasting, J. P., John, J. G., Blanton, C., McHugh, C., Nikonov, S., Radhakrishnan, A., Rand, K., Zadeh, N. T., Balaji, V., Durachta, J., Dupuis, C., Menzel, R., Robinson, T., Underwood, S., Vahlenkamp, H., Dunne, K. A., Gauthier, P. P., Ginoux, P., Griffies, S. M., Hallberg, R., Harrison, M., Hurlin, W., Malyshev, S., Naik, V., Paulot, F., Paynter, D. J., Ploshay, J., Reichl, B. G., Schwarzkopf, D. M., Seman, C. J., Silvers, L., Wyman, B., Zeng, Y., Adcroft, A., Dunne, J. P., Dussin, R., Guo, H., He, J., Held, I. M., Horowitz, L. W., Lin, P., Milly, P., Shevliakova, E., Stock, C., Winton, M., Wittenberg, A. T., Xie, Y., and Zhao, M.: NOAA-GFDL GFDL-ESM4 model output prepared for CMIP6 CMIP historical, https://doi.org/10.22033/ESGF/CMIP6.8597, 2018.

Landrum, L. and Holland, M.: Extremes become routine in an emerging new Arctic, Nat. Clim. Change, 10, 1–8, https://doi.org/10.1038/s41558-020-0892-z, 2020.

Lawrence, D. M., Slater, A. G., Tomas, R. A., Holland, M. M., and Deser, C.: Accelerated Arctic land warming and permafrost degradation during rapid sea ice loss, Geophys. Res. Lett., 35, L11506, https://doi.org/10.1029/2008GL033985, 2008.

Lee, W.-L. and Liang, H.-C.: AS-RCEC TaiESM1.0 model output prepared for CMIP6 CMIP historical, https://doi.org/10.22033/ESGF/CMIP6.9755, 2020a.

Lee, W.-L. and Liang, H.-C.: AS-RCEC TaiESM1.0 model output prepared for CMIP6 ScenarioMIP ssp126, https://doi.org/10.22033/ESGF/CMIP6.9806, 2020b.

Lee, W.-L. and Liang, H.-C.: AS-RCEC TaiESM1.0 model output prepared for CMIP6 ScenarioMIP ssp585, https://doi.org/10.22033/ESGF/CMIP6.9823, 2020c.

Lin, X., Massonnet, F., Fichefet, T., and Vancoppenolle, M.: SITool (v1.0) – a new evaluation tool for large-scale sea ice simulations: application to CMIP6 OMIP, Geosci. Model Dev., 14, 6331–6354, https://doi.org/10.5194/gmd-14-6331-2021, 2021.

McGraw, M. C., Blanchard-Wrigglesworth, E., Clancy, R. P., and Bitz, C. M.: Understanding the Forecast Skill of Rapid Arctic Sea Ice Loss on Subseasonal Time Scales, J. Climate, 35, 1179–1196, https://doi.org/10.1175/JCLI-D-21-0301.1, 2022.

Meredith, M., Sommerkorn, M., Cassotta, S., Derksen, C., Ekaykin, A., Hollowed, A., Kofinas, G., Mackintosh, A., Melbourne-Thomas, J., Muelbert, M., Ottersen, G., Pritchard, H., and Schuur, E.: Polar Regions, in: IPCC Special Report on the Ocean and Cryosphere in a Changing Climate, edited by: Pörtner, H.-O., Roberts, D., Masson-Delmotte, V., Zhai, P., Tignor, M., Poloczanska, E., Mintenbeck, K., Alegría, A., Nicolai, M., Okem, A., Petzold, J., Rama, B., and Weyer, N. M., Cambridge University Press, Cambridge, UK and New York, NY, USA, 203–320, https://doi.org/10.1017/9781009157964.005, 2019.

Mioduszewski, J. R., Vavrus, S., Wang, M., Holland, M., and Landrum, L.: Past and future interannual variability in Arctic sea ice in coupled climate models, The Cryosphere, 13, 113–124, https://doi.org/10.5194/tc-13-113-2019, 2019.

Notz, D.: Sea-ice extent and its trend provide limited metrics of model performance, The Cryosphere, 8, 229–243, https://doi.org/10.5194/tc-8-229-2014, 2014.

Olonscheck, D., Suarez-Gutierrez, L., Milinski, S., Beobide-Arsuaga, G., Baehr, J., Fröb, F., Ilyina, T., Kadow, C., Krieger, D., Li, H., Marotzke, J., Plésiat, E., Schupfner, M., Wachsmann, F., Wallberg, L., Wieners, K.-H., and Brune, S.: The New Max Planck Institute Grand Ensemble With CMIP6 Forcing and High-Frequency Model Output, J. Adv. Model. Earth Sy., 15, e2023MS003790, https://doi.org/10.1029/2023MS003790, 2023.

Onarheim, I. H., Eldevik, T., Smedsrud, L. H., and Stroeve, J. C.: Seasonal and Regional Manifestation of Arctic Sea Ice Loss, J. Climate, 31, 4917–4932, https://doi.org/10.1175/JCLI-D-17-0427.1, 2018.

O'Neill, B. C., Tebaldi, C., van Vuuren, D. P., Eyring, V., Friedlingstein, P., Hurtt, G., Knutti, R., Kriegler, E., Lamarque, J.-F., Lowe, J., Meehl, G. A., Moss, R., Riahi, K., and Sanderson, B. M.: The Scenario Model Intercomparison Project (ScenarioMIP) for CMIP6, Geosci. Model Dev., 9, 3461–3482, https://doi.org/10.5194/gmd-9-3461-2016, 2016.

Paquin, J.-P., Döscher, R., Koenigk, T., and Sushama, L.: Causes and consequences of mid-21st-century rapid ice loss events simulated by the Rossby centre regional atmosphere-ocean model, Tellus A, 65, 19110, https://doi.org/10.3402/tellusa.v65i0.19110, 2013.

Polar Science Center: PIOMAS Arctic Sea Ice Volume Reanalysis version 2.1, Polar Science Center [data set], http://psc.apl.uw.edu/research/projects/arctic-sea-ice-volume-anomaly/data/, last access: 11 August 2025.

Ridley, J., Menary, M., Kuhlbrodt, T., Andrews, M., and Andrews, T.: MOHC HadGEM3-GC31-LL model output prepared for CMIP6 CMIP historical, https://doi.org/10.22033/ESGF/CMIP6.6109, 2019a.

Ridley, J., Menary, M., Kuhlbrodt, T., Andrews, M., and Andrews, T.: MOHC HadGEM3-GC31-MM model output prepared for CMIP6 CMIP historical, https://doi.org/10.22033/ESGF/CMIP6.6112, 2019b.

Rieke, O., Årthun, M., and Dörr, J. S.: Rapid sea ice changes in the future Barents Sea, The Cryosphere, 17, 1445–1456, https://doi.org/10.5194/tc-17-1445-2023, 2023.

Rong, X.: CAMS CAMS-CSM1.0 model output prepared for CMIP6 ScenarioMIP SSP126, https://doi.org/10.22033/ESGF/CMIP6.11046, 2019a.

Rong, X.: CAMS CAMS-CSM1.0 model output prepared for CMIP6 ScenarioMIP SSP585, https://doi.org/10.22033/ESGF/CMIP6.11052, 2019b.

Rong, X.: CAMS CAMS_CSM1.0 model output prepared for CMIP6 CMIP historical, https://doi.org/10.22033/ESGF/CMIP6.9754, 2019c.

Rosenblum, E. and Eisenman, I.: Sea Ice Trends in Climate Models Only Accurate in Runs with Biased Global Warming, J. Climate, 30, 6265–6278, https://doi.org/10.1175/JCLI-D-16-0455.1, 2017.

Schupfner, M., Wieners, K.-H., Wachsmann, F., Steger, C., Bittner, M., Jungclaus, J., Früh, B., Pankatz, K., Giorgetta, M., Reick, C., Legutke, S., Esch, M., Gayler, V., Haak, H., de Vrese, P., Raddatz, T., Mauritsen, T., von Storch, J.-S., Behrens, J., Brovkin, V., Claussen, M., Crueger, T., Fast, I., Fiedler, S., Hagemann, S., Hohenegger, C., Jahns, T., Kloster, S., Kinne, S., Lasslop, G., Kornblueh, L., Marotzke, J., Matei, D., Meraner, K., Mikolajewicz, U., Modali, K., Müller, W., Nabel, J., Notz, D., Peters-von Gehlen, K., Pincus, R., Pohlmann, H., Pongratz, J., Rast, S., Schmidt, H., Schnur, R., Schulzweida, U., Six, K., Stevens, B., Voigt, A., and Roeckner, E.: DKRZ MPI-ESM1.2-HR model output prepared for CMIP6 ScenarioMIP SSP126, https://doi.org/10.22033/ESGF/CMIP6.4397, 2019a.

Schupfner, M., Wieners, K.-H., Wachsmann, F., Steger, C., Bittner, M., Jungclaus, J., Früh, B., Pankatz, K., Giorgetta, M., Reick, C., Legutke, S., Esch, M., Gayler, V., Haak, H., de Vrese, P., Raddatz, T., Mauritsen, T., von Storch, J.-S., Behrens, J., Brovkin, V., Claussen, M., Crueger, T., Fast, I., Fiedler, S., Hagemann, S., Hohenegger, C., Jahns, T., Kloster, S., Kinne, S., Lasslop, G., Kornblueh, L., Marotzke, J., Matei, D., Meraner, K., Mikolajewicz, U., Modali, K., Müller, W., Nabel, J., Notz, D., Peters-von Gehlen, K., Pincus, R., Pohlmann, H., Pongratz, J., Rast, S., Schmidt, H., Schnur, R., Schulzweida, U., Six, K., Stevens, B., Voigt, A., and Roeckner, E.: DKRZ MPI-ESM1.2-HR model output prepared for CMIP6 ScenarioMIP SSP585, https://doi.org/10.22033/ESGF/CMIP6.4403, 2019b.

Schweiger, A., Lindsay, R., Zhang, J., Steele, M., Stern, H., and Kwok, R.: Uncertainty in modeled Arctic sea ice volume, J. Geophys. Res.-Oceans, 116, C00D06, https://doi.org/10.1029/2011JC007084, 2011.

Screen, J., Deser, C., and Sun, L.: Projected changes in regional climate extremes arising from Arctic sea ice loss, Environ. Res. Lett., 10, 084006, https://doi.org/10.1088/1748-9326/10/8/084006, 2015.

Seferian, R.: CNRM-CERFACS CNRM-ESM2-1 model output prepared for CMIP6 CMIP historical, https://doi.org/10.22033/ESGF/CMIP6.4068, 2018.

Seland, Ø., Bentsen, M., Oliviè, D. J. L., Toniazzo, T., Gjermundsen, A., Graff, L. S., Debernard, J. B., Gupta, A. K., He, Y., Kirkevåg, A., Schwinger, J., Tjiputra, J., Aas, K. S., Bethke, I., Fan, Y., Griesfeller, J., Grini, A., Guo, C., Ilicak, M., Karset, I. H. H., Landgren, O. A., Liakka, J., Moseid, K. O., Nummelin, A., Spensberger, C., Tang, H., Zhang, Z., Heinze, C., Iversen, T., and Schulz, M.: NCC NorESM2-LM model output prepared for CMIP6 CMIP historical, https://doi.org/10.22033/ESGF/CMIP6.8036, 2019a.

Seland, Ø., Bentsen, M., Oliviè, D. J. L., Toniazzo, T., Gjermundsen, A., Graff, L. S., Debernard, J. B., Gupta, A. K., He, Y., Kirkevåg, A., Schwinger, J., Tjiputra, J., Aas, K. S., Bethke, I., Fan, Y., Griesfeller, J., Grini, A., Guo, C., Ilicak, M., Karset, I. H. H., Landgren, O. A., Liakka, J., Moseid, K. O., Nummelin, A., Spensberger, C., Tang, H., Zhang, Z., Heinze, C., Iversen, T., and Schulz, M.: NCC NorESM2-LM model output prepared for CMIP6 ScenarioMIP ssp126, https://doi.org/10.22033/ESGF/CMIP6.8248, 2019b.

Seland, Ø., Bentsen, M., Oliviè, D. J. L., Toniazzo, T., Gjermundsen, A., Graff, L. S., Debernard, J. B., Gupta, A. K., He, Y., Kirkevåg, A., Schwinger, J., Tjiputra, J., Aas, K. S., Bethke, I., Fan, Y., Griesfeller, J., Grini, A., Guo, C., Ilicak, M., Karset, I. H. H., Landgren, O. A., Liakka, J., Moseid, K. O., Nummelin, A., Spensberger, C., Tang, H., Zhang, Z., Heinze, C., Iversen, T., and Schulz, M.: NCC NorESM2-LM model output prepared for CMIP6 ScenarioMIP ssp585, https://doi.org/10.22033/ESGF/CMIP6.8319, 2019c.

Senftleben, D., Lauer, A., and Karpechko, A.: Constraining Uncertainties in CMIP5 Projections of September Arctic Sea Ice Extent with Observations, J. Climate, 33, 1487–1503, https://doi.org/10.1175/JCLI-D-19-0075.1, 2020.

Serreze, M. C. and Barry, R. G.: Processes and impacts of Arctic amplification: A research synthesis, Global Planet. Change, 77, 85–96, https://doi.org/10.1016/j.gloplacha.2011.03.004, 2011.

Serreze, M. C., Barrett, A. P., Stroeve, J. C., Kindig, D. N., and Holland, M. M.: The emergence of surface-based Arctic amplification, The Cryosphere, 3, 11–19, https://doi.org/10.5194/tc-3-11-2009, 2009.

Shen, Z., Duan, A., Li, D., and Li, J.: Assessment and Ranking of Climate Models in Arctic Sea Ice Cover Simulation: From CMIP5 to CMIP6, J. Climate, 34, 3609–3627, https://doi.org/10.1175/JCLI-D-20-0294.1, 2021.

Shiogama, H., Abe, M., and Tatebe, H.: MIROC MIROC6 model output prepared for CMIP6 ScenarioMIP SSP126, https://doi.org/10.22033/ESGF/CMIP6.5743, 2019a.

Shiogama, H., Abe, M., and Tatebe, H.: MIROC MIROC6 model output prepared for CMIP6 ScenarioMIP SSP585, https://doi.org/10.22033/ESGF/CMIP6.5771, 2019b.

Shiogama, H., Tatebe, H., Hayashi, M., Abe, M., Arai, M., Koyama, H., Imada, Y., Kosaka, Y., Ogura, T., and Watanabe, M.: MIROC6 Large Ensemble (MIROC6-LE): experimental design and initial analyses, Earth Syst. Dynam., 14, 1107–1124, https://doi.org/10.5194/esd-14-1107-2023, 2023.

Shu, Q., Wang, Q., Song, Z., Qiao, F., Zhao, J., Chu, M., and Li, X.: Assessment of Sea Ice Extent in CMIP6 With Comparison to Observations and CMIP5, Geophys. Res. Lett., 47, e2020GL087965, https://doi.org/10.1029/2020GL087965, 2020.

SIMIP Community: Arctic Sea Ice in CMIP6, Geophys. Res. Lett., 47, e2019GL086749, https://doi.org/10.1029/2019GL086749, 2020.

Stroeve, J. and Meier, W. N.: Sea Ice Trends and Climatologies from SMMR and SSM/I-SSMIS, NSIDC-0192, Version 3, NASA National Snow and Ice Data Center Distributed Active Archive Center [data set], https://doi.org/10.5067/IJ0T7HFHB9Y6, 2018.

Stroeve, J. and Notz, D.: Insights on past and future sea-ice evolution from combining observations and models, Global Planet. Change, 135, 119–132, https://doi.org/10.1016/j.gloplacha.2015.10.011, 2015.

Stroeve, J. and Notz, D.: Changing state of Arctic sea ice across all seasons, Environ. Res. Lett., 13, 103001, https://doi.org/10.1088/1748-9326/aade56, 2018.

Swart, N. C., Fyfe, J. C., Hawkins, E., Kay, J. E., and Jahn, A.: Influence of internal variability on Arctic sea-ice trends, Nat. Clim. Change, 5, 86–89, https://doi.org/10.1038/nclimate2483, 2015.

Swart, N. C., Cole, J. N., Kharin, V. V., Lazare, M., Scinocca, J. F., Gillett, N. P., Anstey, J., Arora, V., Christian, J. R., Jiao, Y., Lee, W. G., Majaess, F., Saenko, O. A., Seiler, C., Seinen, C., Shao, A., Solheim, L., von Salzen, K., Yang, D., Winter, B., and Sigmond, M.: CCCma CanESM5 model output prepared for CMIP6 CMIP historical, https://doi.org/10.22033/ESGF/CMIP6.3610, 2019a.

Swart, N. C., Cole, J. N., Kharin, V. V., Lazare, M., Scinocca, J. F., Gillett, N. P., Anstey, J., Arora, V., Christian, J. R., Jiao, Y., Lee, W. G., Majaess, F., Saenko, O. A., Seiler, C., Seinen, C., Shao, A., Solheim, L., von Salzen, K., Yang, D., Winter, B., and Sigmond, M.: CCCma CanESM5 model output prepared for CMIP6 ScenarioMIP SSP126, https://doi.org/10.22033/ESGF/CMIP6.3683, 2019b.

Swart, N. C., Cole, J. N., Kharin, V. V., Lazare, M., Scinocca, J. F., Gillett, N. P., Anstey, J., Arora, V., Christian, J. R., Jiao, Y., Lee, W. G., Majaess, F., Saenko, O. A., Seiler, C., Seinen, C., Shao, A., Solheim, L., von Salzen, K., Yang, D., Winter, B., and Sigmond, M.: CCCma CanESM5 model output prepared for CMIP6 ScenarioMIP SSP585, https://doi.org/10.22033/ESGF/CMIP6.3696, 2019c.

Swart, N. C., Cole, J. N. S., Kharin, V. V., Lazare, M., Scinocca, J. F., Gillett, N. P., Anstey, J., Arora, V., Christian, J. R., Hanna, S., Jiao, Y., Lee, W. G., Majaess, F., Saenko, O. A., Seiler, C., Seinen, C., Shao, A., Sigmond, M., Solheim, L., von Salzen, K., Yang, D., and Winter, B.: The Canadian Earth System Model version 5 (CanESM5.0.3), Geosci. Model Dev., 12, 4823–4873, https://doi.org/10.5194/gmd-12-4823-2019, 2019d.

Tachiiri, K., Abe, M., Hajima, T., Arakawa, O., Suzuki, T., Komuro, Y., Ogochi, K., Watanabe, M., Yamamoto, A., Tatebe, H., Noguchi, M. A., Ohgaito, R., Ito, A., Yamazaki, D., Ito, A., Takata, K., Watanabe, S., and Kawamiya, M.: MIROC MIROC-ES2L model output prepared for CMIP6 ScenarioMIP SSP126, https://doi.org/10.22033/ESGF/CMIP6.5742, 2019a.

Tachiiri, K., Abe, M., Hajima, T., Arakawa, O., Suzuki, T., Komuro, Y., Ogochi, K., Watanabe, M., Yamamoto, A., Tatebe, H., Noguchi, M. A., Ohgaito, R., Ito, A., Yamazaki, D., Ito, A., Takata, K., Watanabe, S., and Kawamiya, M.: MIROC MIROC-ES2L model output prepared for CMIP6 ScenarioMIP SSP585, https://doi.org/10.22033/ESGF/CMIP6.5770, 2019b.

Tang, Y., Rumbold, S., Ellis, R., Kelley, D., Mulcahy, J., Sellar, A., Walton, J., and Jones, C.: MOHC UKESM1.0-LL model output prepared for CMIP6 CMIP historical, https://doi.org/10.22033/ESGF/CMIP6.6113, 2019.

Tatebe, H. and Watanabe, M.: MIROC MIROC6 model output prepared for CMIP6 CMIP historical, https://doi.org/10.22033/ESGF/CMIP6.5603, 2018.

Tatebe, H., Ogura, T., Nitta, T., Komuro, Y., Ogochi, K., Takemura, T., Sudo, K., Sekiguchi, M., Abe, M., Saito, F., Chikira, M., Watanabe, S., Mori, M., Hirota, N., Kawatani, Y., Mochizuki, T., Yoshimura, K., Takata, K., O'ishi, R., Yamazaki, D., Suzuki, T., Kurogi, M., Kataoka, T., Watanabe, M., and Kimoto, M.: Description and basic evaluation of simulated mean state, internal variability, and climate sensitivity in MIROC6, Geosci. Model Dev., 12, 2727–2765, https://doi.org/10.5194/gmd-12-2727-2019, 2019.

Taylor, P. C., Cai, M., Hu, A., Meehl, J., Washington, W., and Zhang, G. J.: A Decomposition of Feedback Contributions to Polar Warming Amplification, J. Climate, 26, 7023–7043, https://doi.org/10.1175/JCLI-D-12-00696.1, 2013.

Voldoire, A.: CMIP6 simulations of the CNRM-CERFACS based on CNRM-CM6-1 model for CMIP experiment historical, https://doi.org/10.22033/ESGF/CMIP6.4066, 2018.

Voldoire, A.: CNRM-CERFACS CNRM-CM6-1-HR model output prepared for CMIP6 CMIP historical, https://doi.org/10.22033/ESGF/CMIP6.4067, 2019a.

Voldoire, A.: CNRM-CERFACS CNRM-CM6-1-HR model output prepared for CMIP6 ScenarioMIP SSP585, https://doi.org/10.22033/ESGF/CMIP6.4225, 2019b.

Voldoire, A.: CNRM-CERFACS CNRM-CM6-1 model output prepared for CMIP6 ScenarioMIP SSP126, https://doi.org/10.22033/ESGF/CMIP6.4184, 2019c.

Voldoire, A.: CNRM-CERFACS CNRM-CM6-1 model output prepared for CMIP6 ScenarioMIP SSP585, https://doi.org/10.22033/ESGF/CMIP6.4224, 2019d.

Voldoire, A.: CNRM-CERFACS CNRM-ESM2-1 model output prepared for CMIP6 ScenarioMIP ssp126, https://doi.org/10.22033/ESGF/CMIP6.4186, 2019e.

Voldoire, A.: CNRM-CERFACS CNRM-ESM2-1 model output prepared for CMIP6 ScenarioMIP ssp585, https://doi.org/10.22033/ESGF/CMIP6.4226, 2019f.

Voldoire, A.: CNRM-CERFACS CNRM-CM6-1-HR model output prepared for CMIP6 ScenarioMIP ssp126, https://doi.org/10.22033/ESGF/CMIP6.4185, 2020.

Wang, Z., Walsh, J., Szymborski, S., and Peng, M.: Rapid Arctic Sea Ice Loss on the Synoptic Time Scale and Related Atmospheric Circulation Anomalies, J. Climate, 33, 1597–1617, https://doi.org/10.1175/JCLI-D-19-0528.1, 2020.

Wassmann, P., Duarte, C. M., Agusti, S., and Sejr, M. K.: Footprints of climate change in the Arctic marine ecosystem, Global Change Biol., 17, 1235–1249, https://doi.org/10.1111/j.1365-2486.2010.02311.x, 2011.

Watts, M., Maslowski, W., Lee, Y. J., Kinney, J. C., and Osinski, R.: A Spatial Evaluation of Arctic Sea Ice and Regional Limitations in CMIP6 Historical Simulations, J. Climate, 34, 6399–6420, https://doi.org/10.1175/JCLI-D-20-0491.1, 2021.

WCRP: CMIP6, WCRP [data set], https://esgf-node.ipsl.upmc.fr/search/cmip6-ipsl/, last access: 11 August 2025.

Wieners, K.-H., Giorgetta, M., Jungclaus, J., Reick, C., Esch, M., Bittner, M., Gayler, V., Haak, H., de Vrese, P., Raddatz, T., Mauritsen, T., von Storch, J.-S., Behrens, J., Brovkin, V., Claussen, M., Crueger, T., Fast, I., Fiedler, S., Hagemann, S., Hohenegger, C., Jahns, T., Kloster, S., Kinne, S., Lasslop, G., Kornblueh, L., Marotzke, J., Matei, D., Meraner, K., Mikolajewicz, U., Modali, K., Müller, W., Nabel, J., Notz, D., Peters-von Gehlen, K., Pincus, R., Pohlmann, H., Pongratz, J., Rast, S., Schmidt, H., Schnur, R., Schulzweida, U., Six, K., Stevens, B., Voigt, A., and Roeckner, E.: MPI-M MPI-ESM1.2-LR model output prepared for CMIP6 ScenarioMIP SSP126, https://doi.org/10.22033/ESGF/CMIP6.6690, 2019a.

Wieners, K.-H., Giorgetta, M., Jungclaus, J., Reick, C., Esch, M., Bittner, M., Gayler, V., Haak, H., de Vrese, P., Raddatz, T., Mauritsen, T., von Storch, J.-S., Behrens, J., Brovkin, V., Claussen, M., Crueger, T., Fast, I., Fiedler, S., Hagemann, S., Hohenegger, C., Jahns, T., Kloster, S., Kinne, S., Lass-

lop, G., Kornblueh, L., Marotzke, J., Matei, D., Meraner, K., Mikolajewicz, U., Modali, K., Müller, W., Nabel, J., Notz, D., Peters-von Gehlen, K., Pincus, R., Pohlmann, H., Pongratz, J., Rast, S., Schmidt, H., Schnur, R., Schulzweida, U., Six, K., Stevens, B., Voigt, A., and Roeckner, E.: MPI-M MPI-ESM1.2-LR model output prepared for CMIP6 ScenarioMIP SSP585, https://doi.org/10.22033/ESGF/CMIP6.6705, 2019b.

Wieners, K.-H., Giorgetta, M., Jungclaus, J., Reick, C., Esch, M., Bittner, M., Legutke, S., Schupfner, M., Wachsmann, F., Gayler, V., Haak, H., de Vrese, P., Raddatz, T., Mauritsen, T., von Storch, J.-S., Behrens, J., Brovkin, V., Claussen, M., Crueger, T., Fast, I., Fiedler, S., Hagemann, S., Hohenegger, C., Jahns, T., Kloster, S., Kinne, S., Lasslop, G., Kornblueh, L., Marotzke, J., Matei, D., Meraner, K., Mikolajewicz, U., Modali, K., Müller, W., Nabel, J., Notz, D., Peters-von Gehlen, K., Pincus, R., Pohlmann, H., Pongratz, J., Rast, S., Schmidt, H., Schnur, R., Schulzweida, U., Six, K., Stevens, B., Voigt, A., and Roeckner, E.: MPI-M MPI-ESM1.2-LR model output prepared for CMIP6 CMIP historical, https://doi.org/10.22033/ESGF/CMIP6.6595, 2019c.

Wu, T., Chu, M., Dong, M., Fang, Y., Jie, W., Li, J., Li, W., Liu, Q., Shi, X., Xin, X., Yan, J., Zhang, F., Zhang, J., Zhang, L., and Zhang, Y.: BCC BCC-CSM2MR model output prepared for CMIP6 CMIP historical, https://doi.org/10.22033/ESGF/CMIP6.2948, 2018.

Wyser, K., Koenigk, T., Fladrich, U., Fuentes-Franco, R., Karami, M. P., and Kruschke, T.: The SMHI Large Ensemble (SMHI-LENS) with EC-Earth3.3.1, Geosci. Model Dev., 14, 4781–4796, https://doi.org/10.5194/gmd-14-4781-2021, 2021.

Xin, X., Wu, T., Shi, X., Zhang, F., Li, J., Chu, M., Liu, Q., Yan, J., Ma, Q., and Wei, M.: BCC BCC-CSM2MR model output prepared for CMIP6 ScenarioMIP SSP126, https://doi.org/10.22033/ESGF/CMIP6.3028, 2019a.

Xin, X., Wu, T., Shi, X., Zhang, F., Li, J., Chu, M., Liu, Q., Yan, J., Ma, Q., and Wei, M.: BCC BCC-CSM2MR model output prepared for CMIP6 ScenarioMIP SSP585, https://doi.org/10.22033/ESGF/CMIP6.3050, 2019b.

Yukimoto, S., Koshiro, T., Kawai, H., Oshima, N., Yoshida, K., Urakawa, S., Tsujino, H., Deushi, M., Tanaka, T., Hosaka, M., Yoshimura, H., Shindo, E., Mizuta, R., Ishii, M., Obata, A., and Adachi, Y.: MRI MRI-ESM2.0 model output prepared for CMIP6 CMIP historical, https://doi.org/10.22033/ESGF/CMIP6.6842, 2019a.

Yukimoto, S., Koshiro, T., Kawai, H., Oshima, N., Yoshida, K., Urakawa, S., Tsujino, H., Deushi, M., Tanaka, T., Hosaka, M., Yoshimura, H., Shindo, E., Mizuta, R., Ishii, M., Obata, A., and Adachi, Y.: MRI MRI-ESM2.0 model output prepared for CMIP6 ScenarioMIP SSP126, https://doi.org/10.22033/ESGF/CMIP6.6909, 2019b.

Yukimoto, S., Koshiro, T., Kawai, H., Oshima, N., Yoshida, K., Urakawa, S., Tsujino, H., Deushi, M., Tanaka, T., Hosaka, M., Yoshimura, H., Shindo, E., Mizuta, R., Ishii, M., Obata, A., and Adachi, Y.: MRI MRI-ESM2.0 model output prepared for CMIP6 ScenarioMIP SSP585, https://doi.org/10.22033/ESGF/CMIP6.6929, 2019c.

Zhang, J. and Rothrock, D. A.: Modeling Global Sea Ice with a Thickness and Enthalpy Distribution Model in Generalized Curvilinear Coordinates, Mon. Weather Rev., 131, 845–861, https://doi.org/10.1175/1520-0493(2003)131<0845:MGSIWA>2.0.CO;2, 2003.

Ziehn, T., Chamberlain, M., Lenton, A., Law, R., Bodman, R., Dix, M., Wang, Y., Dobrohotoff, P., Srbinovsky, J., Stevens, L., Vohralik, P., Mackallah, C., Sullivan, A., O'Farrell, S., and Druken, K.: CSIRO ACCESS-ESM1.5 model output prepared for CMIP6 CMIP historical, https://doi.org/10.22033/ESGF/CMIP6.4272, 2019a.

Ziehn, T., Chamberlain, M., Lenton, A., Law, R., Bodman, R., Dix, M., Wang, Y., Dobrohotoff, P., Srbinovsky, J., Stevens, L., Vohralik, P., Mackallah, C., Sullivan, A., O'Farrell, S., and Druken, K.: CSIRO ACCESS-ESM1.5 model output prepared for CMIP6 ScenarioMIP SSP126, https://doi.org/10.22033/ESGF/CMIP6.4320, 2019b.

Ziehn, T., Chamberlain, M., Lenton, A., Law, R., Bodman, R., Dix, M., Wang, Y., Dobrohotoff, P., Srbinovsky, J., Stevens, L., Vohralik, P., Mackallah, C., Sullivan, A., O'Farrell, S., and Druken, K.: CSIRO ACCESS-ESM1.5 model output prepared for CMIP6 ScenarioMIP SSP585, https://doi.org/10.22033/ESGF/CMIP6.4333, 2019c.

Ziehn, T., Chamberlain, M., Law, R., Lenton, A., Bodman, R., Dix, M., Stevens, L., Wang, Y., and Srbinovsky, J.: The Australian Earth System Model: ACCESS-ESM1.5, Journal of Southern Hemisphere Earth Systems Science, 70, 193–214, https://doi.org/10.1071/ES19035, 2020.